

SN 2015U: A Rapidly Evolving and Luminous Type Ibn Supernova

Isaac Shivvers,^{1*} WeiKang Zheng,¹ Jon Mauerhan,¹ Io K. W. Kleiser,^{1,2}
 Patrick L. Kelly,¹ Jeffrey M. Silverman,³ Melissa L. Graham,¹
 Alexei V. Filippenko,¹ Sahana Kumar,¹ Schuyler D. Van Dyk⁴

¹*Department of Astronomy, University of California, Berkeley, CA 94720-3411, USA*

²*Department of Astronomy, California Institute of Technology, Pasadena, CA 91125, USA*

³*Department of Astronomy, University of Texas at Austin, Austin, TX 78712, USA*

⁴*Spitzer Science Center/Caltech, Mail Code 220-6, Pasadena, CA 91125, USA*

Submitted to MNRAS

ABSTRACT

Supernova (SN) 2015U (also known as PSN J07285387+3349106) was discovered in NGC 2388 on 2015 Feb. 11. A rapidly evolving and luminous event, it showed hydrogen-free spectra dominated by relatively narrow helium P-Cygni spectral features and it was classified as a SN Ibn. In this paper we present photometric, spectroscopic, and spectropolarimetric observations of SN 2015U, including a Keck/DEIMOS spectrum (resolution ≈ 5000) which fully resolves the optical emission and absorption features. We find that SN 2015U is best understood via models of shock breakout from extended and dense circumstellar material (CSM), likely created by a history of mass loss from the progenitor with an extreme outburst within ~ 1 – 2 yr of core collapse (but we do not detect any outburst in our archival imaging of NGC 2388). We argue that the high luminosity of SN 2015U was powered not through ^{56}Ni decay but via the deposition of kinetic energy into the ejecta/CSM shock interface, and we place an upper limit on the amount of ^{56}Ni synthesized by SN 2015U: $M(^{56}\text{Ni}) < 0.019 M_{\odot}$. Though our analysis is hampered by strong host-galaxy dust obscuration (which likely exhibits multiple components), our dataset makes SN 2015U one of the best-studied Type Ibn supernovae and provides a bridge of understanding to other rapidly fading transients, both luminous and relatively faint.

Key words: supernovae: individual: SN 2015U – stars: mass loss

1 INTRODUCTION

Core-collapse supernovae (SNe) are luminous explosions that mark the end of a massive star’s life. These SNe are differentiated from their thermonuclear counterparts (Type Ia SNe) and are grouped into classes via spectral and photometric analyses (e.g., Filippenko 1997). The major core-collapse subclasses include SNe IIP and IIL, events which show strong hydrogen throughout their evolution and respectively do or do not exhibit a hydrogen-recombination plateau in their light curves (though the distinction between SNe IIP and IIL may be less clear than previously thought; e.g., Arcavi et al. 2012; Anderson et al. 2014; Sanders et al. 2015). SNe Ib and Ic (often called stripped-envelope SNe) are core-collapse events that show no hydrogen in their spectra and (for SNe Ic and broad-lined SNe Ic) no helium; they

(along with the intermediate SNe IIb, which exhibit very little hydrogen) are commonly understood to arise from progenitor stars that have lost all or most of their hydrogen (and perhaps helium) envelopes prior to core collapse, though the detailed connections between progenitors and SN observables remain somewhat uncertain (e.g., Matheson et al. 2001; Drout et al. 2011; Bianco et al. 2014; Modjaz et al. 2014; Liu et al. 2015; Dessart et al. 2015).

A subset of SNe reveal signatures of a dense shroud of circumstellar material (CSM) surrounding their progenitors at the time of explosion. For hydrogen-rich events, relatively narrow lines (full width at half-maximum intensity [FWHM] $\lesssim 1000 \text{ km s}^{-1}$) from this interaction with the CSM are often detected; these objects have been dubbed SNe IIn (e.g., Schlegel 1990; Filippenko 1991). This interaction can provide a significant luminosity boost (as has been observed for superluminous SNe IIn; e.g., Gal-Yam 2012). CSM interaction occurs in some hydrogen-poor SNe as well. SNe Ia-

* E-mail: ishivvers@berkeley.edu

CSM are thermonuclear events that exhibit relatively narrow features (usually $H\alpha$ emission) caused by interaction with hydrogen-rich CSM (though the underlying SN ejecta are hydrogen-poor; e.g., [Silverman et al. 2013b,a](#)). A small number of stripped-envelope SNe have been found to exhibit the spectral signatures of CSM interaction. SNe Ibn (e.g., [Foley et al. 2007](#); [Pastorello et al. 2008](#)) show relatively narrow helium lines in their spectra but no hydrogen, and they can be quite heterogeneous in their photometric evolution (e.g., [Pastorello et al. 2016](#)), while the remarkable SN 2014C appeared to be a normal SN Ib at peak brightness but then began interacting with hydrogen-rich CSM only few months later ([Milisavljevic et al. 2015](#)).

In addition to the examples of interaction with dense CSM described above, indications of very short-lived interaction with CSM have been discovered through “flash spectroscopy” of very young SNe of various types (e.g., [Gal-Yam et al. 2014](#); [Shivvers et al. 2015](#); [Khazov et al. 2016](#)). These examples exist on a continuum of CSM densities with the strongly interacting events described above; they require much less CSM and their observables at peak generally align with those of “normal” events.

Here we present the results of our observational campaign to study SN 2015U: a remarkable and very well-studied SN Ibn. It was discovered in NGC 2388 by the Lick Observatory Supernova Search (LOSS) and the 0.76 m Katzman Automatic Imaging Telescope (KAIT; [Filippenko et al. 2001](#)) on 2015 Feb. 11 (all dates and times reported herein are in UT). Note that, because the official International Astronomical Union name was not assigned until November of 2015 ([Kumar et al. 2015](#)), this event has also been discussed in the literature under the name PSN J07285387+3349106. [Ochner et al. \(2015\)](#) classified it as a young SN Ibn based upon spectra obtained on Feb. 18, which showed a blue continuum and relatively narrow He I emission features (see also [Kumar et al. 2015](#)). [Tsvetkov et al. \(2015\)](#) present *BVRI* photometry of SN 2015U starting Feb. 17, showing that it has one of the fastest decline rates known (similar to those SNe 2002bj, 2005ek, and 2010X) and is remarkably luminous (though SN 2015U is significantly obscured by an uncertain amount of dust in the host galaxy). [Pastorello et al. \(2015\)](#) present additional photometry and low-resolution spectra of this event and describe SN 2015U within the context of SNe Ibn (e.g., [Foley et al. 2007](#); [Pastorello et al. 2008, 2016](#)).

In this paper we present photometric, spectroscopic, and spectropolarimetric observations of SN 2015U, including one epoch of relatively high-resolution Keck DEIMOS spectroscopy ($R = \lambda/\delta\lambda \approx 5000$), enabling us to study the narrow-line features in detail. We show that SN 2015U is similar to several other SNe from the heterogeneous SN Ibn class, and that it shares many features with the rapid and luminous transients discovered in the Pan-STARRS1 (PS1) archives ([Drouot et al. 2014](#)), those found in the SuperNova Legacy Survey (SNLS) archives ([Arcavi et al. 2015](#)), and with a few other rapidly fading SNe from the literature. SN 2015U offers valuable insights into the physics of the poorly observed class of rapidly fading SNe.

2 OBSERVATIONS

2.1 Photometry

SN 2015U was first detected by KAIT on Feb. 11.24 at 18.06 ± 0.15 mag in an unfiltered image¹. An unfiltered image taken the night before (Feb. 10.30) shows no source to a limit of ~ 18.37 mag. We began acquiring multiband photometry (*BVRI* and *clear*) starting Feb. 14 with KAIT and the 1 m Nickel telescope at Lick Observatory. We used a set of 8 Nickel images with clear detections of SN 2015U and with good astrometric solutions for the field to calculate an updated position: $\alpha = 07^h28^m53.89^s$, $\delta = +33^\circ 49' 10.52''$ (J2000), offset from the centre of the galaxy by $\sim 6''$. We believe this position to be accurate within $0.15''$ or better — the positions we measured for the SN exhibit a scatter of $\sigma_\alpha = 0.08''$ and $\sigma_\delta = 0.03''$ across 8 images.

NGC 2388 and the location of SN 2015U were imaged in the near-infrared by the *Hubble Space Telescope (HST)* in 2004, but there are no coincident sources detected in the archival images. Though SN 2015U is one of the nearest SNe Ibn to date ([Pastorello et al. 2016](#)), it is still much too distant for our nondetection to place interesting constraints on a putative progenitor. Under our Cycle 23 Snapshot program with *HST*’s Wide Field Camera 3 (WFC3; GO-14149, PI Filippenko), we obtained images of the SN location on 2016 Feb. 14 (1 yr post explosion) through the *F555W* (710 s) and *F814W* (780 s) filters. SN 2015U is not detected in these images, but we do find that it exploded on the trailing edge of the approaching spiral arm of NGC 2388, in a region with several probable dust lanes and a generally clumpy appearance. NGC 2388 is a strongly star-forming and massive galaxy — [Pereira-Santaella et al. \(2015\)](#) calculate an ongoing star-formation rate of $\sim 40^{+9}_{-22} M_\odot \text{ yr}^{-1}$ and a total stellar mass of $10^{11.0 \pm 0.1} M_\odot$ — but SN 2015U is not obviously associated with the brightest star-forming regions of the galaxy. Figure 1 displays a Nickel *V*-band detection of SN 2015U and our *HST F555W* image of the SN site.

[Ganeshalingam et al. \(2010\)](#) describe our photometric observing program at Lick in detail. KAIT and Nickel images were reduced using our image-reduction pipeline ([Ganeshalingam et al. 2010](#)). Point-spread-function photometry was then performed using DAOPHOT ([Stetson 1987](#)) from the IDL Astronomy User’s Library.² Instrumental magnitudes were calibrated to several nearby stars from the Sloan Digital Sky Survey, transformed into the Landolt system using the empirical prescription presented by Robert Lupton.³ Figure 2 shows our light curves of SN 2015U; upon publication the data will be available for download from the Berkeley SuperNova DataBase (SNDB; [Silverman et al. 2012](#)).⁴

We measure the time of peak of SN 2015U’s brightness in each passband of our Nickel+KAIT photometry by fitting a low-order polynomial to the light curve within the first week (first 10 days for *I*) and use Monte Carlo Markov Chain (MCMC) methods to estimate our uncertainties. In

¹ The KAIT *clear* passband is similar to the *R* band but broader. For more details and transformations to standard passbands, see [Riess et al. \(1999\)](#) and [Li et al. \(2003\)](#).

² <http://idlastro.gsfc.nasa.gov/>

³ <http://www.sdss.org/dr7/algorithms/sdssUBVRITransform.html>

⁴ <http://heracles.astro.berkeley.edu/sndb/>

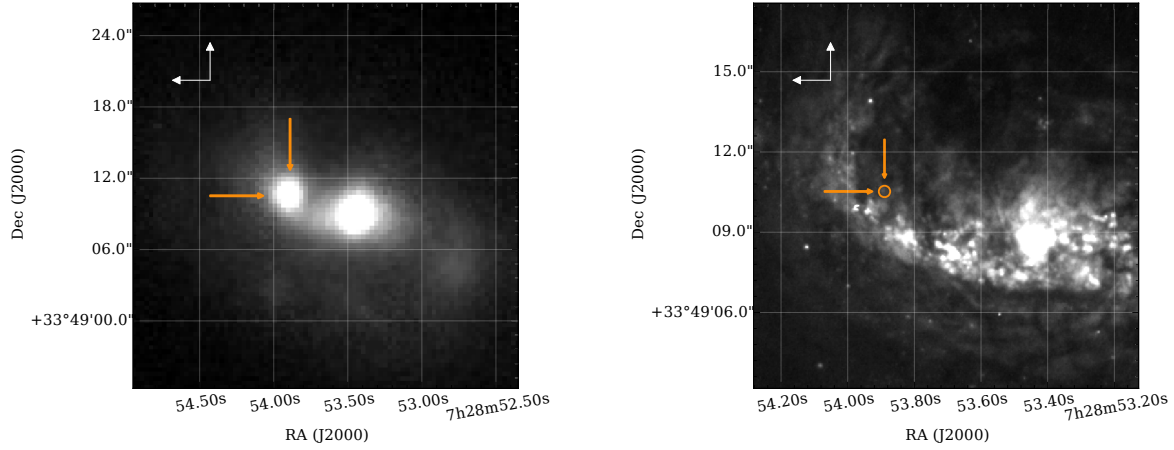


Figure 1. At left is a detection of SN 2015U by the Lick Nickel 1 m telescope through the V -band filter; at right is an *HST* image observed through the $F555W$ filter on 2016 Feb. 14 (1 yr post-explosion). Both images show the location of the SN with orange arrows, and the size of our 5σ position error is marked with a circle in the right panel. There are no detected sources near the SN position in the *HST* image.

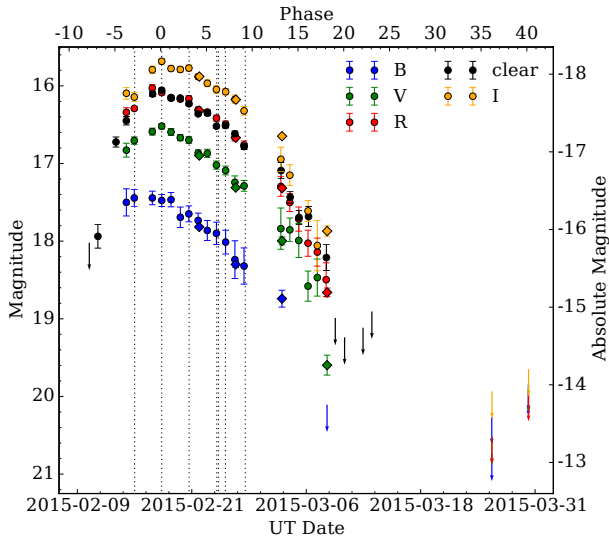


Figure 2. The $BVRI$ and *clear* passband light curves of SN 2015U after correcting for Milky Way (MW) dust absorption but not for the host absorption. KAIT data are indicated by circles and Nickel data by diamonds. The dates of our spectral observations are marked by dotted vertical lines. The phase relative to the V -band peak is shown along the top while the absolute magnitude is shown on the right. Because these absolute magnitudes have not been corrected for significant but uncertain dust absorption arising within the host galaxy, they can be taken as lower limits on the luminosity of SN 2015U.

Modified Julian Day (MJD), we find $t_V^{\max} = 57071.1 \pm 0.23$, $t_R^{\max} = 57071.6 \pm 0.47$, and $t_I^{\max} = 57072.4 \pm 0.19$ (our data do not constrain the B -band peak well). Throughout our analysis we present phases relative to the V -band peak. NGC 2388 is at a redshift of $z_{\text{host}} = 0.013790 \pm 0.000017$ (NED; de Vaucouleurs et al. 1991), which (assuming cosmological parameters $H_0 = 71 \text{ km s}^{-1} \text{ Mpc}^{-1}$, $\Omega_m = 0.27$, and $\Omega_\Lambda = 0.73$) translates into a luminosity distance of 58.9 Mpc (Wright 2006)

and a distance modulus of 33.85 mag, which we use for all absolute-magnitude corrections.

2.2 Spectroscopy

We began a spectral monitoring campaign of SN 2015U on 2015 Feb. 15, obtaining six spectra with the Kast double spectrograph (Miller & Stone 1993) on the Shane 3 m telescope at Lick Observatory and one spectrum with the DEIMOS spectrograph (Faber et al. 2003) on the Keck II 10 m telescope. Details of our spectral observations are listed in Table 1, and all reductions and calibrations were performed with standard tools and methods, including IRAF routines and custom Python and IDL code⁵ (e.g., Matheson et al. 2000; Pérez & Granger 2007; Silverman et al. 2012).

All spectra were taken at or near the parallactic angle (Filippenko 1982), and the amount of galaxy flux falling into the slit varied as a function of seeing and the slit orientation on the sky. For the spectra which included a large amount of host-galaxy flux (Feb. 18, 21, and 24), we extract a spectrum from a region of the galaxy that does not include any SN 2015U flux, perform a median-filter smoothing to obtain the galaxy continuum, and then subtract it from our spectra, after determining a best-fit galaxy scaling coefficient by comparing synthetic photometry to the (template-subtracted) multiband photometry observed the same night. We do not attempt to remove the narrow (unresolved) galaxy emission features, so our spectra show varying degrees of narrow-line contamination from the host (including $H\alpha$, $H\beta$, and $[SII]$).

We renormalise each spectrum to match our template-subtracted V or R -band photometry (depending on the spectral wavelength coverage) after linearly interpolating the photometry to the time of spectral observation. Figure 3 shows our total-flux spectra of SN 2015U. Upon publication all spectra will be available to download from the Berke-

⁵ <https://github.com/ishivvers/TheKastShiv>

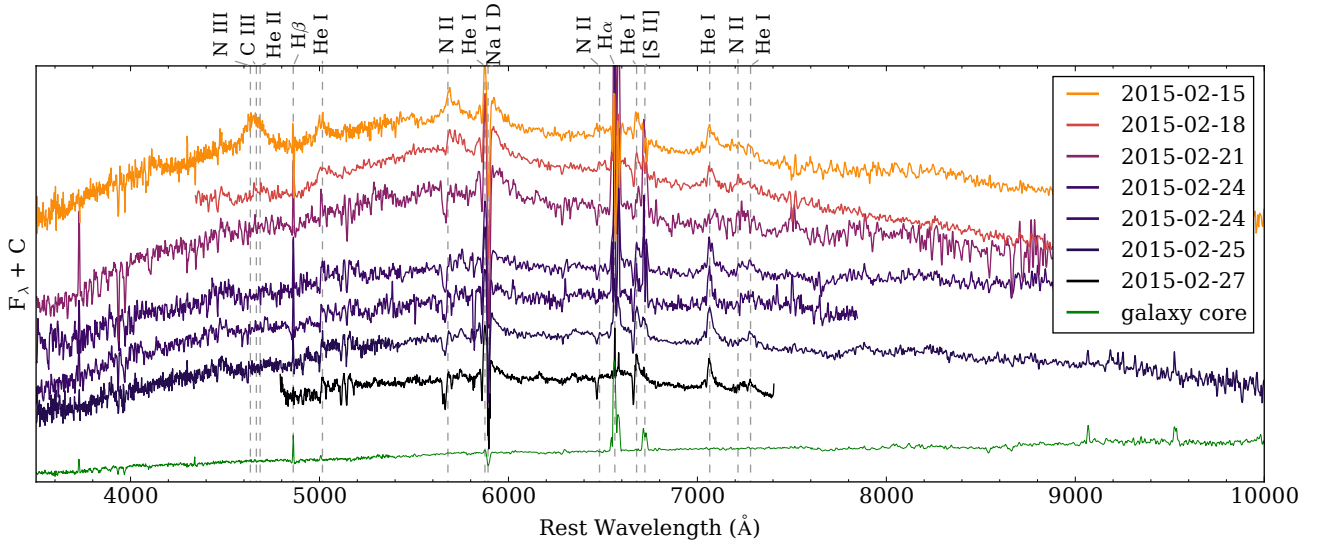


Figure 3. The spectral sequence of SN 2015U. This figure shows the spectral evolution after dereddening to correct for MW dust absorption but not for the host absorption. On the bottom, we show an extraction of NGC 2388’s core, taken from a Kast spectrum obtained on Feb. 15. Contamination from the host galaxy’s strong emission lines is apparent in some spectra; we indicate H α , H β , and [S II] $\lambda\lambda$ 6716, 6731, as well as the host’s Na I D absorption.

ley SNDB and the Weizmann Interactive Supernova Data REPOSITORY (WiseREP; Yaron & Gal-Yam 2012).⁶

Using narrow H α host emission in our DEIMOS spectrum we measure a line-of-sight redshift at the SN’s location: $z_{\text{SN}} = 0.013161 \pm 0.000005$, a difference of $\sim 200 \text{ km s}^{-1}$ from the published redshift of the host galaxy — consistent with the SN’s position on the approaching arm of this spiral galaxy.

2.3 Spectropolarimetry

Three epochs of spectropolarimetry were obtained of SN 2015U near peak brightness utilising the dual-beam polarimetry mode of the Lick Kast spectrograph. The orientation of the slit on the sky was always set to a position angle of 180° (i.e., aligned north-south), and exposures of 900s were obtained at each of four waveplate positions (0:0, 45:0, 22:5, and 67:5). On each night, several waveplate sequences were performed and coadded. Flatfield and arc-lamp spectra were obtained immediately after each sequence without moving the telescope.

For polarimetric calibrations, the low-polarization standard stars BD+32°3739 and BD+05°2618 were observed to verify the low instrumental polarization of the Kast spectrograph. We constrained the average fractional Stokes Q and U values to $< 0.1\%$. By observing the above unpolarized standard stars through a 100% polarizing filter we determined that the polarimetric response is so close to 100% that no correction was necessary. Finally, we obtained the instrumental polarization position-angle curve and used it to correct the data. We observed the high-polarization stars

HD 19820, BD +59°389, and V1Cygl12 to obtain the zero-point of the polarization position angle on the sky (θ) and to determine the accuracy of polarimetric measurements, which were generally consistent with previously published values within $\Delta P < 0.05\%$ and $\Delta\theta < 1^\circ$. All spectropolarimetric reductions and calculations were performed using the methods described by Mauerhan et al. (2015, and references therein), and we define the polarimetric parameters in the same manner as those authors (Stokes parameters q and u , debiased polarization P , and sky position angle θ).

To probe the Galactic component of interstellar polarization (ISP) along the line of sight toward SN 2015U, we used the method of spectroscopic parallax to select three stars within 1° of separation from the source and measured their integrated V -band polarization (P) and position angle (θ). For HD 58221 we obtained $P = 0.28\% \pm 0.01\%$, $\theta = 13.0^\circ \pm 0.6^\circ$; for HD 58726, $P = 0.50\% \pm 0.01\%$, $\theta = 24.8^\circ \pm 0.3^\circ$; and for HD 59291, $P = 0.24\% \pm 0.01\%$, $\theta = 16.3^\circ \pm 0.7^\circ$ (uncertainties are statistical). We interpret the significantly higher value of P for HD 58726 (A0 V spectral type) as being caused by some intrinsic polarization for that star, so we used the average values of the other two stars (0.25%, 14.3°) to calculate the associated Serkowski-Whittet form (Serkowski et al. 1975; Whittet et al. 1992), assuming a total-to-selective extinction ratio of $R_V = 3.1$ and that the polarization peaks at 5500 \AA , values appropriate for the Milky Way (MW). The resulting curve was subtracted from the SN 2015U data to remove the small but nonnegligible Galactic component of ISP. The above observations (along with calibration observations of the low-polarization standard star HD 14069 and the high-polarization standards HD 245310 and HD 25443) were taken with the Kast spectrograph on 2015 Sep. 21.

⁶ <http://wiserep.weizmann.ac.il/>

Table 1. Journal of Spectroscopic Observations

UT Date	Type ^a	Tel./Instr.	Wavelength (Å)	Resolution (Å)	Exp. (s)	Observer ^b	Reducer ^b
2015-02-15.256	F	Shane/Kast	3440–10,870	2	1200	IS	IS
2015-02-18.211	F	Shane/Kast	4400–9880	2	2400	WZ	IS
2015-02-21.207	F	Shane/Kast	3500–10,500	2	1200	WZ	IS
2015-02-21.313	S	Shane/Kast	4500–10,000	16	4 × 4 × 900 ^c	WZ	JM
2015-02-24.224	F	Shane/Kast	3500–10,500	2	1200	WZ	IS
2015-02-24.322	S	Shane/Kast	4500–10,000	16	3 × 4 × 900 ^c	WZ	JM
2015-02-24.414	F	Shane/Kast	3500–7875	1	1800	WZ	IS
2015-02-25.171	F	Shane/Kast	3500–10,500	2	1200	MG	MG
2015-02-25.301	S	Shane/Kast	4500–10,000	16	5 × 4 × 900 ^c	MG	JM
2015-02-27.34	F	Keck/DEIMOS	4850–7510	0.3	1200	PK	IS

^a F: total flux; S: spectropolarimetry

^b Observers and data reducers are indicated with their initials. IS: Isaac Shivvers; WZ: WeiKang Zheng; JM: Jon Mauerhan; MG: Melissa Graham; PK: Patrick Kelly.

^c All spectropolarimetry was obtained by rotating multiple times through four waveplate positions; see §2.3.

3 ANALYSIS

3.1 Dust Corrections

All observations of SN 2015U are heavily affected by an obscuring screen of dust present in the host galaxy, NGC 2388. Because the treatment of dust corrections affects much of the following discussion, we start by describing our efforts to understand, characterise, and correct for the effects of the host-galaxy dust. First, however, we correct for MW dust along the line of sight using the dust maps of [Schlafly & Finkbeiner \(2011\)](#), $E(B - V) = 0.0498$ mag) and assuming $R_V = 3.1$ ([Cardelli et al. 1989](#)).

[Ochner et al. \(2015\)](#) note that a significant amount of host-galaxy reddening is apparent in their classification spectrum, with an estimated $E(B - V) = 1.0$ mag based upon the Na I D feature. Our higher-resolution DEIMOS spectrum from Feb. 27 reveals complex Na I D absorption near the host redshift (we examine the structure of this feature in §3.2.3). We measure the equivalent width (EW) of the entire absorption complex to be 9.1 ± 0.15 Å — well outside the empirical relations of [Poznanski et al. \(2012\)](#) and similar previous efforts, which show that the Na I D lines saturate and lose their predictive power above a total EW of ~ 2 Å and $E(B - V) \approx 1.0$ mag. This indicates that the reddening toward SN 2015U likely exhibits $E(B - V) > 1.0$ mag, if the dust in NGC 2388 is similar to that in our MW.

[Pastorello et al. \(2015\)](#) measure an Na I D EW of 6.5 ± 0.5 Å from their spectra; we tentatively suggest that the discrepancy between their value and ours is caused by different choices made when defining the local continuum. Figure 6 shows that the Na I D components fall on the red wing of the He I emission line, even at early times. However, if one instead defines the local continuum based upon the overall flux-density level (a reasonable choice if the emission-line wings were not detected), one obtains Na I D EW values similar to those of [Pastorello et al. \(2015\)](#).

We next examined the 5870.5 Å diffuse interstellar band (DIB). This feature is one of the strongest DIBs; it has long been known to correlate with extinction in the MW when the Na I D feature is saturated (e.g., [Herbig 1995](#); [Fried-](#)

[man et al. 2011](#); [Lan et al. 2015](#)), and [Phillips et al. \(2013\)](#) show a clear correlation between this feature and the reddening toward SNe Ia produced by host-galaxy dust. We do not detect this feature, and our spectra have insufficient signal-to-noise ratio (SNR) to place strong constraints on the dust using our nondetection. We also examined modeled estimates for the amount of dust obscuring the bulk of stars in the host galaxy NGC 2388 ([Pereira-Santaella et al. 2015](#)), and we determined the same value at the location of the SN (within $\sim 1''$ on the sky) by measuring the Balmer ratio implied by the H α and H β galaxy lines present in our DEIMOS spectrum (e.g., [Brocklehurst 1971](#)). We estimate $E(B - V) \approx 0.56$ and 1.1 mag, respectively, toward the average star in NGC 2388’s core and the average star near the explosion site of SN 2015U. Although this does not provide a measure of the line-of-sight reddening toward SN 2015U specifically, it does provide valuable context about the dust content of NGC 2388.

Additional information is available to us through the spectropolarimetry: as we describe in §3.2.4, the peak of the polarization spectrum (λ_{\max}) of NGC 2388’s ISM is blueward of 4600 Å. The shapes of the polarization law and the dust-extinction law are related within the MW (e.g., [Serkowski et al. 1975](#); [Clayton & Mathis 1988](#)). Using $R_V = (-0.29 \pm 0.74) + (6.67 \pm 1.17) \lambda_{\max}$ from [Clayton & Mathis \(1988\)](#), with λ_{\max} in μm , our measurement of $\lambda_{\max} < 0.46 \mu\text{m}$ implies $R_V < 2.8 \pm 0.9$. However, note that [Patat et al. \(2015\)](#) show the polarization properties of the host-galaxy dust obscuring several well-studied and reddened SNe Ia to be remarkably different from those of the dust in our MW.

Finally, we model SN 2015U as a blackbody emitter obscured behind a simple screen of dust in the host galaxy and fit for the parameters of that dust via comparisons with our multiband photometry at three epochs (pre-maximum, maximum, and post-maximum). Our spectra show that the emission from SN 2015U is roughly that of a blackbody obscured by dust, at least at optical wavelengths (unlike most SNe, which display spectra consisting of prominent and overlapping features with sometimes strong line blanketing), and in §3.5 we discuss why one would expect roughly black-

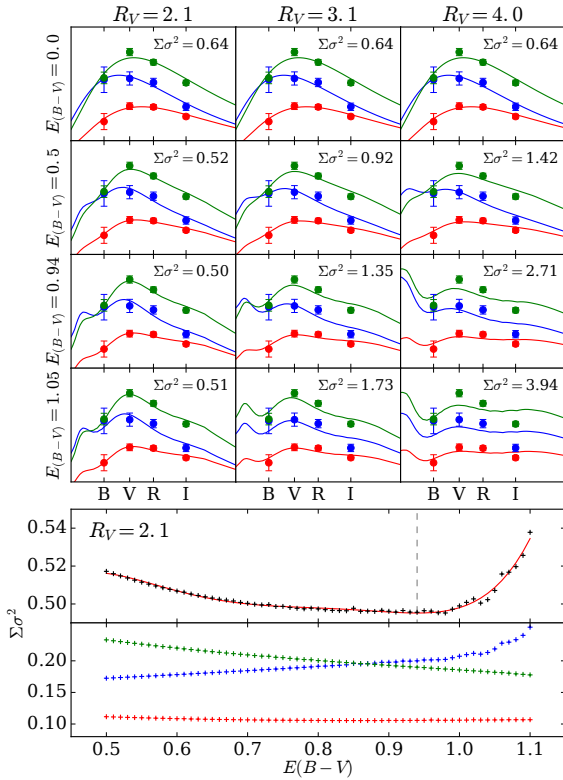


Figure 4. In the top panel, we fit reddened blackbodies to our photometry of SN 2015U at three epochs (blue, Feb. 14.35; green, Feb. 18.21; red, Feb. 27.21) after correcting for MW absorption and assuming various values for R_V and $E(B-V)$ within NGC 2388. For many data points, the measurement errors are smaller than the plotted symbol. The weighted sum of squared differences ($\Sigma\sigma^2$) between observed photometric points and synthetic photometry of a blackbody is shown in the upper right of each plot; lower values indicate a better agreement across all epochs. In the bottom panel, we show $\Sigma\sigma^2$ as a function of $E(B-V)$ for $R_V = 2.1$ in black as well as $\Sigma\sigma^2$ broken down by individual epochs, coloured as above. $R_V = 2.1$ and $E(B-V) = 0.94^{+0.1}_{-0.4}$ mag (marked with a dashed line in the bottom panel) are the preferred values. In many panels a blue feature is introduced into the reddened blackbody spectrum by the wavelength dependency of the MW’s reddening law, but our spectral data provide no clear evidence for or against such a feature in the spectra of SN 2015U.

body emission from SN 2015U. We use PySynphot⁷ and assume the dust is described by the empirical extinction law of Cardelli et al. (1989) — by varying the parameters R_V and $E(B-V)$ we are able to explore a wide variety of dust populations and search for the parameters that produce the best blackbody fits to our photometric data.

Figure 4 shows a comparison between synthetic photometry from PySynphot and the photometry assuming four different values for $E(B-V)$ ranging from 0.0 mag to 1.0 mag and three different reddening laws parameterised by R_V from 2.1 to 4.0 (note that PySynphot only includes a few built-in options for R_V ; we explore the most relevant of them here). For every combination of R_V and $E(B-V)$ we perform a

weighted least-squares fit to determine the best-fit temperature and luminosity of the source blackbody and we list the weighted sum of squared differences ($\Sigma\sigma^2$) for each. Figure 4 shows that a nonzero amount of host-galaxy reddening correction makes the fits worse for $R_V = 3.1$ and 4.0 — in those cases the photometric data prefer a blackbody with no dust. However, the spectra clearly show a nonthermal rolloff at blue wavelengths (see Figure 3), and so there must be a significant amount of dust absorption within NGC 2388. If we instead adopt $R_V = 2.1$, a grid search over $E(B-V)$ values indicates a best fit at $E(B-V) \approx 0.94$ mag. As Figure 5 shows, dereddening the spectra for this reddening law appears to correct the blue rolloff. Figure 4 shows that $\Sigma\sigma^2$ increases above $E(B-V) = 1.0$ and below $E(B-V) = 0.6$, but between those values $\Sigma\sigma^2$ is only weakly dependent upon $E(B-V)$. We therefore use Figure 4 to estimate our error bars: $E(B-V) = 0.94^{+0.1}_{-0.4}$ mag. A similar approach was taken by Pastorello et al. (2015), who compared the colour curves of SN 2015U to the intrinsic colour curves of other SNe Ibn to obtain $E(B-V)_{\text{tot}} = 0.81 \pm 0.21$ mag (assuming $R_V = 3.1$). However, as they note, the SN Ibn subclass is remarkably heterogeneous, and it is not clear whether the physics governing those colour curves is the same for all members.

Given the above discussion, we adopt $R_V = 2.1$ and $E(B-V) = 0.94^{+0.1}_{-0.4}$ mag. The large EWs measured from the NaID and the odd absorption feature complex indicate that a simple analysis of those features cannot be trusted. Studies of the integrated galaxy flux and the Balmer decrement measured from our spectrum show that the bulk of NGC 2388’s stellar mass is strongly obscured, and our spectropolarimetric data indicate that SN 2015U itself exploded behind a significant dust screen. The low λ_{max} value in the polarization spectrum and our blackbody fits to the light curves together prefer a relatively wavelength-dependent dust extinction law for NGC 2388 (i.e., $R_V < 3.1$) and $E(B-V) = 0.94^{+0.1}_{-0.4}$ mag — we find this line of reasoning most convincing. The above result is consistent with the $E(B-V) = 0.99 \pm 0.48$ mag adopted by Pastorello et al. (2015), though they assume $R_V = 3.1$. Our determination of the dust properties toward SN 2015U remains uncertain, so we consider a range of plausible reddening corrections throughout the rest of this paper. We find that the extinction toward §3.2.3 does not appear to change over the course of our observations, and we discuss and reject the possibility that a significant fraction of the extinction toward SN 2015U arises from the SN’s CSM rather than the host galaxy’s ISM.

3.2 Spectra

The spectra of SN 2015U show a strong continuum overlain with narrow and intermediate-width emission features. Though our data cover only 12 days of SN 2015U’s evolution, they range from a pre-maximum spectrum to one taken after the SN had faded from peak by ~ 1 mag (see Figure 2). No broad ejecta features became apparent in our spectra throughout that timespan — markedly different behaviour from that of the well-observed, rapidly fading SNe 2002bj, 2005ek, and 2010X (Poznanski et al. 2010; Drout et al. 2013; Kasliwal et al. 2010) and similar to that of the interacting SN 2010jl (e.g., Fransson et al. 2014). Though broad features do not emerge, the continuum temperature shows significant evolution, the narrow emission and absorption features

⁷ <http://ssb.stsci.edu/pysynphot/docs/>

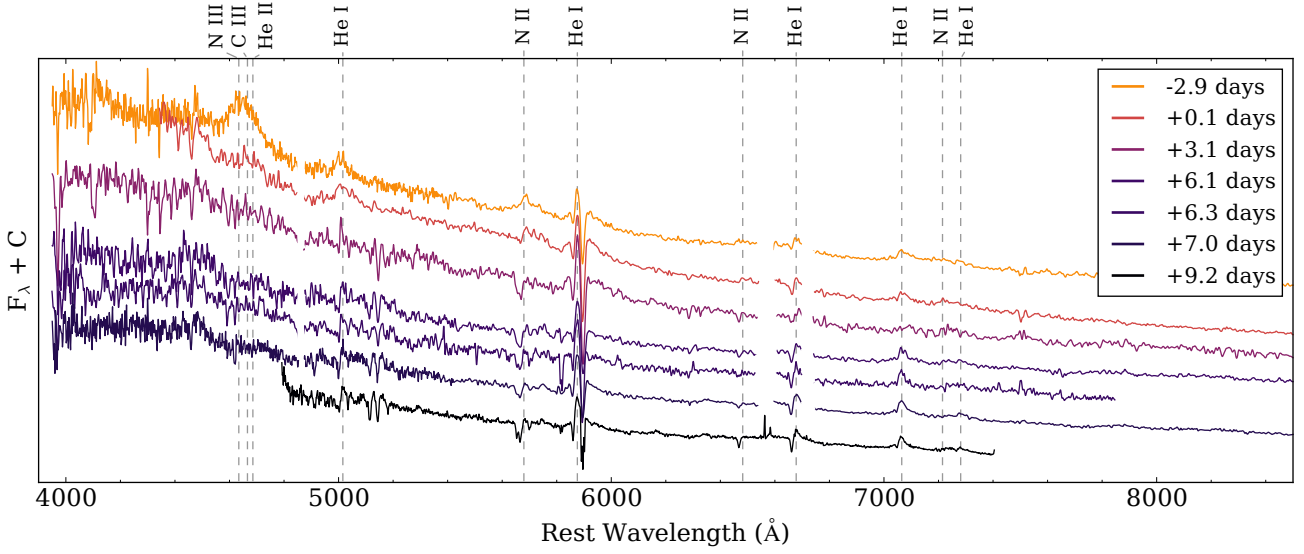


Figure 5. The spectral sequence of SN 2015U after dereddening to correct for MW dust absorption and the (uncertain) host absorption. Phases are listed relative to the V -band peak. We have masked regions of our low-resolution spectra where the host’s narrow emission lines dominate, but we do not mask the NaID absorption features from the MW and the host.

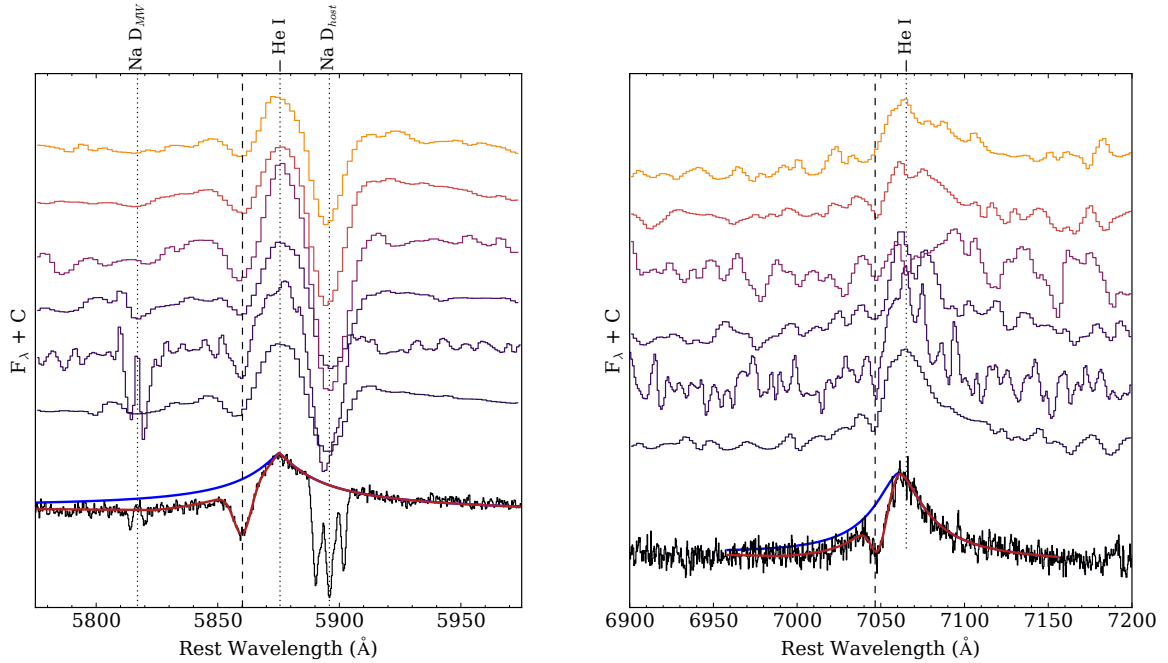


Figure 6. The evolution of the He I $\lambda 5876$ (left) and $\lambda 7065$ (right) lines. The spectra are increasing in time downward on the plot as in Figure 3. The rest wavelength of each line is shown with a dotted line and the absorption component is marked at a blueshift of $v = 789 \text{ km s}^{-1}$ (the mean blueshift of He I lines measured from our DEIMOS spectrum). In the left panel we also mark the host and MW NaID absorption features (see §3.2.3 for a discussion of the host galaxy’s remarkable NaID absorption complex).

evolve, and the relative ionisation states of the detected elements change. No hydrogen is found, but multiple ionisation levels of helium, nitrogen, iron, and perhaps oxygen and carbon are detected, some in both emission and absorption and some in absorption only. Pastorello et al. (2015) also present a series of spectral observations of SN 2015U. Their

data are in good agreement with ours and extend to later epochs, while our (higher-resolution) spectra illustrate new details not apparent previously.

3.2.1 Evolving Line Profiles

The most obvious features in our spectra are emission lines of He I. These lines are centred at the rest wavelength, show a relatively broad base with a full width near zero intensity (FWZI) of $\sim 9000\text{--}10,000\text{ km s}^{-1}$, and are overlain with P-Cygni absorption features blueshifted by $\sim 745\text{ km s}^{-1}$ and with widths of $400\text{--}500\text{ km s}^{-1}$. The wavelengths and widths of these features do not significantly change during the ~ 12 days covered by our spectra. We find that the He I line profiles can be parameterised by a “modified Lorentzian” emission component (where the exponent is allowed to vary) with a suppressed blue wing and an overlain Gaussian absorption component, indicative of recombination lines broadened via electron scattering within the CSM. SN 2015U’s line profiles are very similar to those observed in many SNe IIn but with a faster inferred CSM velocity (see, e.g., the spectra of SN 1998S; Leonard et al. 2000; Anupama et al. 2001; Fasasia et al. 2001; Chugai 2001; Shivvers et al. 2015). Figure 6 shows our best fit to the He I $\lambda 5876$ line using this parameterisation. We also show the unsuppressed Lorentzian feature to emphasise the asymmetry, which arises from the effects of Compton scattering within a wind-like CSM (e.g., Auer & van Blerkom 1972; Hillier 1991; Chugai 2001). The magnitude of the effect scales with the expansion velocity, explaining the strongly asymmetric emission lines of SN 2015U compared to those observed in most SNe IIn.

After He I (and host-galaxy $H\alpha$ and [N II]), the most clearly detected features in our spectra are the N II lines. As Pastorello et al. (2015) note, SN 2015U appears to be the first SN IIn to show these features, though they are commonly found in the spectra of hot stars. In our DEIMOS spectrum we are able to identify nine N II absorption lines (see §3.2.2), and for the strongest of these we track their evolution throughout our spectral series. In our -2.9 and $+0.1$ d spectra, the 5667 \AA and 5676 \AA features are apparent in emission around $v \approx 0\text{ km s}^{-1}$, but they transition into absorption at $v \approx 680\text{ km s}^{-1}$ after maximum light — see Figure 7. The same trend is apparent in the N II features at 6482 \AA and 7215 \AA (Figure 3).

We find a strong emission feature centred around 4650 \AA in our earliest spectrum. In Figure 3 we label it as a blend of N III, C III, and He II, a blend that has been observed and modeled in the spectra of a few other young, interacting SNe (e.g., Gal-Yam et al. 2014; Shivvers et al. 2015). The 4650 \AA emission feature fades rapidly. Given the clear detection of N II at all epochs we believe the identification of N III to be very robust, but whether the blue wing of that emission feature is caused by C III or He II is more difficult to determine. There is abundant helium in SN 2015U, but the energy required to ionise C III is lower than that of He II, and is nearer the ionisation energy of N III ($E_i = 47.44, 47.88,$ and 54.42 eV for N III, C III, and He II, respectively). Discerning between these ions likely requires detailed modeling and is beyond the scope of this paper, and so our identification of carbon in the spectra SN 2015U is only tentative.

3.2.2 Higher Resolution

Our DEIMOS spectrum from Feb. 27 ($R \approx 5000$) reveals fully resolved absorption and emission features from a host of ions in the spectra of SN 2015U; see Figure 8, as well as

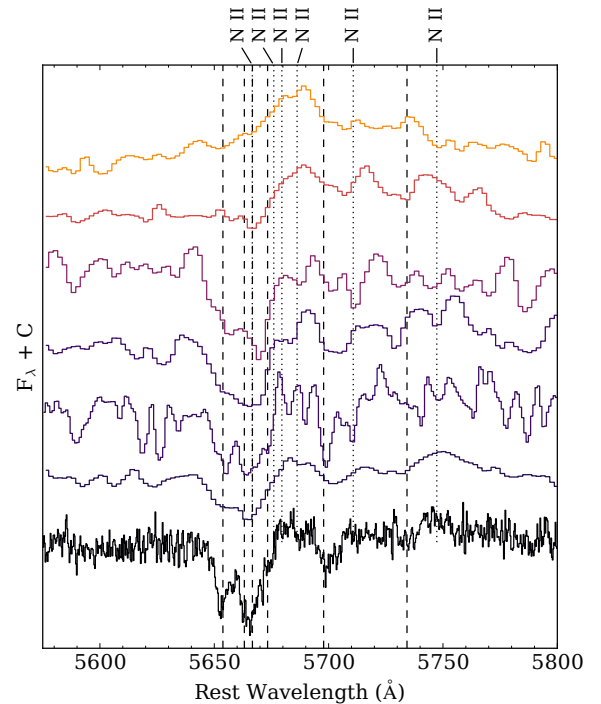


Figure 7. The evolution of the N II lines. The spectra increase in time downward as in Figure 3. Identified N II lines are shown at rest with dotted lines and with a blueshift of $v = 680\text{ km s}^{-1}$ in dashed lines (the mean blueshift of N II lines measured from our DEIMOS spectrum). The emission features marginally detected at $v = 0\text{ km s}^{-1}$ in our earliest spectra evolve into blueshifted absorption lines post-maximum brightness.

Table 2 for their observed properties. We include measured positions and widths for several lines for which we have no good identification; it is especially difficult to differentiate between Fe III ($E_i = 30.651\text{ eV}$) and Fe II ($E_i = 16.20\text{ eV}$).⁸ In our spectrum we find three probable Fe absorption lines between 5115 and 5180 \AA (in the SN rest frame). The stronger two were identified as Fe III by Pastorello et al. (2015), but several known Fe II lines occur at very similar wavelengths. In addition, we find a weaker feature at 5180.3 \AA . NIST lists more than 20 Fe II lines between 5190 and 5200 \AA (implied Doppler velocities of $\sim 560\text{--}1100\text{ km s}^{-1}$), but only one Fe III line within the same range at 5199.08 \AA ($v \approx 1080\text{ km s}^{-1}$). If we assume the observed feature arises from Fe III, then it must be associated with material traveling $\sim 300\text{ km s}^{-1}$ faster than the rest of the CSM — an unlikely scenario. We therefore prefer an identification of Fe II for all three of these features, though we do not present Doppler velocities since they likely arise from several closely spaced lines.

We also find three unidentified emission features in our DEIMOS spectrum that are not from host-galaxy contamination, falling near $5290, 6165,$ and 6340 \AA and exhibiting widths similar to those of the He I lines. None of these is clearly detected in our other spectra or the spectra published

⁸ All ionisation energies and line wavelengths were found through the NIST Atomic Spectra Database (ASD): <http://www.nist.gov/pml/data/asd.cfm>.

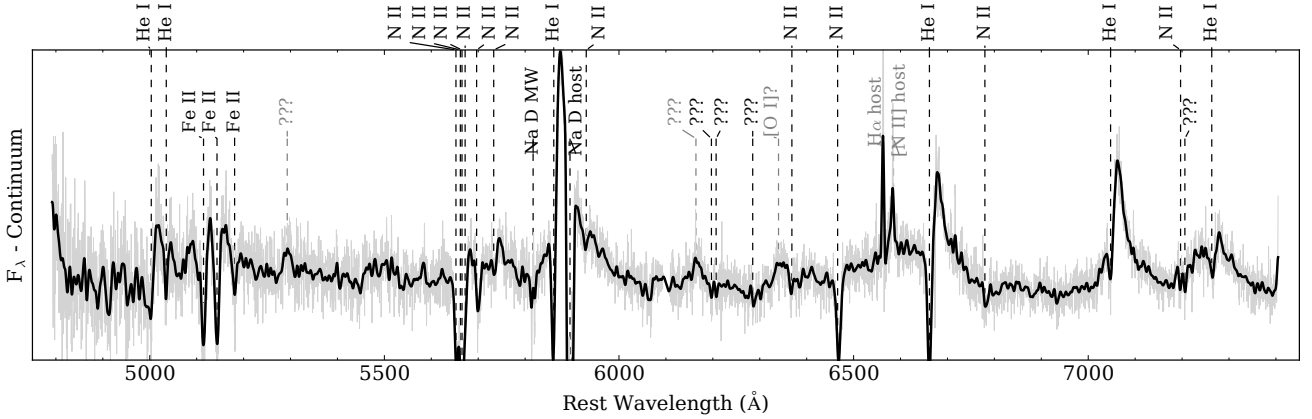


Figure 8. The DEIMOS spectrum from Feb. 27 in detail. A simple polynomial continuum fit has been removed. The full spectrum is shown in grey in the background while the black line displays the spectrum smoothed with a 10 Å Gaussian kernel. Identified emission features are shown with grey dashed lines and text; absorption features are in black. All absorption features are indicated with a 745 km s⁻¹ blueshift but emission features are marked at rest velocity.

Table 2. Absorption Features in the DEIMOS Spectrum

Ion	Rest λ (Å)	Observed λ (Å)	Offset (km s ⁻¹)	FWHM (km s ⁻¹)
He I	5015.7	5002.6	778.8	586.4
He I	5047.7	5034.6	783.2	267.8
He I	5875.6	5860.2	789.2	488.7
He I	6678.2	6661.7	737.2	470.1
He I	7065.2	7047.9	733.7	432.9
He I	7281.3	7265.4	655.9	404.0
N II	5666.6	5653.0	721.4	232.5
N II	5676.0	5665.4	559.2	433.1
N II	5710.8	5699.9	570.4	407.2
N II	5747.3	5734.8	651.6	367.5
N II	6482.1	6468.1	643.4	428.1
N II	5941.6	5927.5	711.5	600.7
N II	6796.6	6781.8	654.2	337.9
N II	7214.7	7195.9	783.5	173.7
N II	6384.3	6366.7	829.6	253.7
Fe II ^a	—	5114.9	—	514.4
Fe II ^a	—	5143.2	—	585.0
Fe II ^a	—	5180.3	—	545.8
?	—	6197.2	—	166.9
?	—	6207.3	—	152.7
?	—	6285.9	—	153.8
?	—	7206.5	—	190.5

Identifications and properties of the absorption features identified in our DEIMOS spectrum (after correcting for $z = 0.013161$). All lines were fit by a Gaussian with a linear approximation to the nearby continuum, and rest wavelengths were downloaded from the NIST ASD. Characteristic error bars are ~ 0.6 Å (30 km s⁻¹) for the observed wavelengths and ~ 1.6 Å for the Gaussian FWHM (85 km s⁻¹), as estimated by calculating the 95% confidence intervals for the N II $\lambda 5711$ line using MCMC techniques.

^a Without more detailed modeling, it is difficult to determine whether Fe II or Fe III is responsible for these features.

by Pastorello et al. (2015, though generally they all exhibit SNRs too low to rule them out). The feature at 6340 Å is suggestive of the [O I] $\lambda\lambda 6300, 6364$ doublet that regularly arises in nebular spectra of stripped-envelope SNe (Types Ib/c; e.g., Filippenko 1997; Matheson 2001), but this identification is only tentative.

3.2.3 The Na D Lines

Our DEIMOS spectrum of SN 2015U reveals a remarkable set of Na D absorption features — see Figure 9. In addition to the MW doublet we find several overlapping lines from NGC 2388 along our sight line, though as we show below,

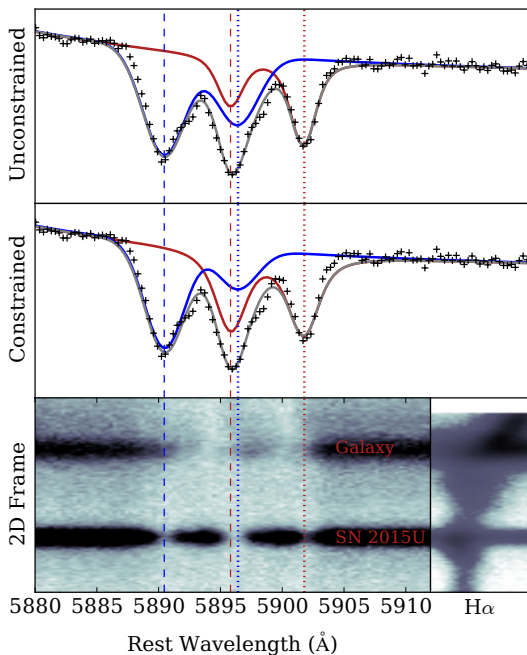


Figure 9. The NaD features in our DEIMOS spectrum of SN 2015U and NGC 2388. The top panel plots the observed spectrum of SN 2015U with our best-fit absorption profiles while the middle panel shows the result after introducing the additional constraint that $D_2/D_1 \geq 1.0$ (see §3.2.3). The shorter-wavelength doublet is shown in blue and the longer-wavelength one in red, with the central wavelengths indicated by dashed and dotted vertical lines for D_2 and D_1 , respectively. Their sum is shown in grey. The bottom panel shows the 2D frame of our DEIMOS observation in this region, including both the light from the host and the SN, as well as a cutout of the $H\alpha$ emission line (plotted with the same Doppler δv per pixel) to indicate the shape of the galaxy’s rotation curve.

there is no evidence that any of these lines originate within the CSM immediately surrounding SN 2015U. The astronomical NaD doublet has been studied in great detail (it was one of the original Fraunhofer lines) and the relative strength of the doublet has long been used to measure the interstellar abundance of neutral sodium: the NaD₂ line is generally observed to be stronger than the D₁ line by a factor ranging from 1.0 to 2.0, for high and low column densities of NaI, respectively (e.g., Strömberg 1948; Nachman & Hobbs 1973; Somerville 1988). The MW NaD doublet in our spectra exhibits the expected behaviour, with an EW ratio of $D_2/D_1 \approx 1.2$, but the host-galaxy lines do not.

There are at least two distinct and overlapping NaD absorption doublets near the host-galaxy’s rest frame in the spectrum of SN 2015U. Figure 9 shows them (as well as model fits) in detail. We model the absorption complex by overlaying the modified Lorentzian emission-line profile (see §3.2.1) with two doublets of Voigt absorption profiles (though we note that some of these lines may be unresolved and saturated). D_1 and D_2 lines from a single doublet are forced to have the same velocity properties and to be separated by 5.97 \AA , but they are allowed independent strengths.

In the top panel of Figure 9 we show the result when we allow the relative strengths of the doublet (i.e., D_2/D_1) to vary freely. In the rest frame of the SN, the bluest doublet falls at $\lambda\lambda 5890.45, 5896.35 \pm 0.066 \text{ \AA}$. This is a blueshift of only $\sim 25 \text{ km s}^{-1}$ from the SN rest frame, and so this doublet is likely to arise from the ISM of NGC 2388 along our sight line to SN 2015U. The second (redder) doublet, however, falls at $\lambda\lambda 5895.80, 5901.69 \pm 0.063 \text{ \AA}$ — redshifted from the SN by almost 300 km s^{-1} , and even redshifted from the galaxy core by more than 100 km s^{-1} . This is within the velocity range of NGC 2388’s rotation curve, but SN 2015U is located well away from the receding spiral arm and the bulk of the galaxy’s receding material (see Figure 1). In addition, the second NaD doublet shows a strength ratio of $D_2/D_1 \approx 0.5$, well outside the commonly observed values of $\sim 1.0\text{--}2.0$ (in contrast, the blue doublet exhibits a reasonable $D_2/D_1 \approx 1.5$).

If, instead, we constrain the doublet ratio to $D_2/D_1 \geq 1.0$, we can also obtain a reasonable fit, though this introduces noticeable discrepancies in the reddest part of the feature — see the middle panel of Figure 9. In addition, this forces the doublet ratio of the bluer doublet outside of the range of normal values: $D_2/D_1 \approx 2.5$. Adding more components to our model fit will not solve this quandary (though the data do show a shoulder on the bluer doublet, suggesting a third absorption component). The implications for the NaI gas (and the dust) in NGC 2388 are not clear.

Given the spectral signatures of dense CSM surrounding SN 2015U, it is natural to wonder whether some of the NaD absorption arises within the local CSM. Variation in the NaD features over the timescale of the SN evolution would be a clear signature of local absorption; however, as Figure 6 shows, no such variation is apparent.

The bottom panel of Figure 9 displays a cutout of the two-dimensional (2D) DEIMOS spectrum around the NaD feature. Both SN 2015U and NGC 2388 are clearly visible, and we also show the rotation curve of the galaxy via a cutout of the $H\alpha$ emission line. The NaD absorption of NGC 2388’s own ISM is seen against the stellar light of the galaxy, and this galactic self-absorption roughly covers the velocity range observed between the two components observed along the line of sight toward SN 2015U. It appears that the anomalous red component described above obscures the host galaxy as well as the SN, providing further evidence that this component is unlikely to arise within the CSM of SN 2015U.

3.2.4 Spectropolarimetry

We did not observe significant evolution in the polarization of SN 2015U between our three epochs, so we coadded all of the data to increase the SNR; the results are illustrated in Figure 10. The polarization spectrum of SN 2015U appears to be dominated by ISP associated with the host galaxy NGC 2388, showing a strong increase in continuum polarization toward shorter wavelengths with a value of $P \approx 2.5\%$ at 4600 \AA and decreasing to $P \approx 1.0\%$ near 7000 \AA . This behaviour is dissimilar to what is typically observed for the MW ISP, which exhibits a peak and turnover near 5500 \AA . Instead, the observed behaviour is reminiscent of the ISP produced by the host galaxies of several SNe Ia, including SNe 1986G, 2006X, 2008fp, and 2014J (Patat et al. 2015, see

their Figure 2). The continuous rise in P beyond the B and U photometric passbands has previously been interpreted as evidence for scattering by dust grains smaller than those characteristic of the MW disk ISM.

Interestingly, we observe a significant wavelength dependence for the position angle (θ), which has a value of $\sim 25^\circ$ at 4600 Å and monotonically trends toward $\sim 10^\circ$ near 7000 Å. In the MW, the ISP’s position angle is generally flat. However, a wavelength dependence in θ has been observed along particular lines of sight toward star-forming regions at distances greater than 0.6 kpc (e.g., Gehrels & Silvester 1965; Coyne & Gehrels 1966), and has been explained as the result of photons traversing multiple clouds or scattering media that exhibit various sizes for the scattering particles as well as various orientations for the interstellar magnetic field.

A similar interpretation is plausible here: along the line of sight within NGC 2388 toward SN 2015U there are likely to be multiple separate components of dusty scattering media having different grain sizes and/or different magnetic field orientations. This possibility is particularly interesting considering the complex superposition of multiple NaID absorption doublets that we see in our high-resolution DEIMOS spectrum. If the continuum flux spectrum of SN 2015U is devoid of broad SN features because of high optical-depth CSM, then one might suspect there also to be a separate and distinct scattering component associated with this CSM, if it is dusty. The subsequent rescattering of this light as it traverses the dusty ISM of the host could provide a means for producing the observed wavelength dependence of θ , if there is a difference in grain sizes between these multiple scattering media. Although this scenario is physically plausible, the spectropolarimetric data cannot discriminate between a CSM+ISM scattering combination and multiple components of host ISM, and our analysis of the total-flux NaID features indicates that they are likely associated with ISM (see §3.2.3).

Finally, there is a line-like feature near 5820 Å which might naively be interpreted as a signature of intrinsic polarization associated with SN 2015U and with the He I / Na I transition. However, the MW NaID doublet falls at the same wavelength. Although relatively weak compared to the redshifted host-galaxy Na D absorption, the results of our spectral arithmetic in the vicinity of this poorly resolved doublet profile might have created a spurious artifact in the final coadded dataset mimicking the shape of a polarized line feature. Indeed, in each individual epoch, the polarized spectra near this feature appear to suffer from systematic noise, so we are reluctant to attribute this feature to the SN itself.

3.3 Photometry

The optical light curves of SN 2015U show that it was a remarkably luminous and rapidly evolving event — Figure 11 shows our photometry corrected for host-galaxy dust reddening. With a peak absolute magnitude of $\lesssim -19$ mag at optical wavelengths, a rise time of $\lesssim 10$ d, a time above half-maximum of $t_{1/2} \approx 12$ d, and a decline rate of nearly 0.2 mag day^{-1} after peak, SN 2015U was more than a magnitude brighter than most stripped-envelope SNe and evolved

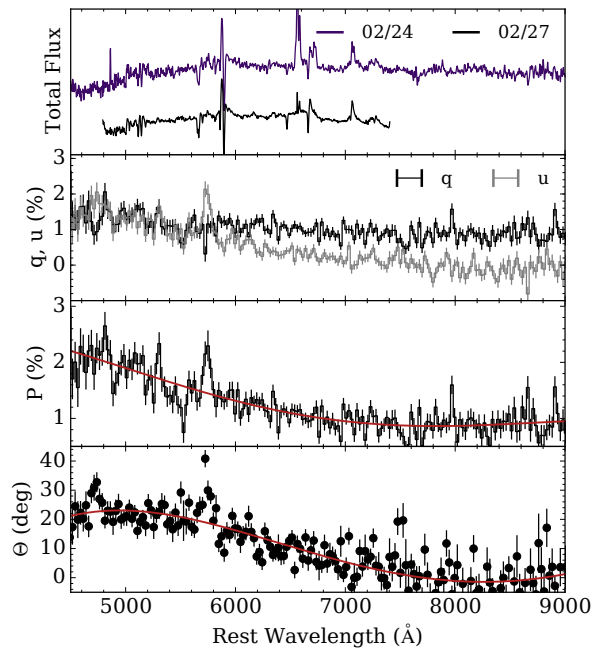


Figure 10. Our spectropolarimetric observations of SN 2015U. From top to bottom: total-flux spectra near V -band peak and in higher-resolution (for visual comparison), q and u Stokes parameters, P with a fourth-order polynomial fit showing the overall trend, and θ with a similar polynomial fit (after discarding outliers). The spectropolarimetric data from three nights of observations have been coadded and binned to 25 Å.

much more rapidly (e.g., Drout et al. 2011; Bianco et al. 2014).

Though the first unfiltered (*clear*) KAIT detection of SN 2015U was on Feb. 11, and it went undetected by KAIT on Feb. 10 (> 18.37 mag), Pastorello et al. (2015) present detections from Feb. 9 and 10 at $R = 18.62 \pm 0.26$ and 18.14 ± 0.30 mag, respectively. Unfortunately, the location does not appear to have been observed in the days prior and there are not deep upper limits constraining the explosion date further. SN 2015U rose quite rapidly, so we adopt a tentative explosion date one day before the first detection published by Pastorello et al. (2015): $t_{\text{exp}} \approx 57062$ MJD (Feb. 8). This provides us with a rise time for SN 2015U of $t_{\text{rise}} \approx 9$ days. Tsvetkov et al. (2015) note that SN 2015U is among the most rapidly evolving SNe known, with a decline rate similar to those of SNe 2002bj, 2005ek, and 2010X. We measure $\Delta M_{15} \approx 2.0$ mag in the R band, but note that the decline rate increases ever more steeply after ~ 10 days post-peak and at all times the bluer passbands decline more rapidly than the red. Simple linear fits indicate the following decline rates before and after +10 d (in mag day^{-1}): $B_{\text{early}} = 0.110 \pm 0.007$, $V_{\text{early}} = 0.099 \pm 0.005$, $V_{\text{late}} = 0.28 \pm 0.07$, $R_{\text{early}} = 0.080 \pm 0.005$, $R_{\text{late}} = 0.267 \pm 0.009$, $I_{\text{early}} = 0.067 \pm 0.006$, and $I_{\text{late}} = 0.26 \pm 0.04$ (uncertainties are statistical, and our data do not constrain the late B -band decline).

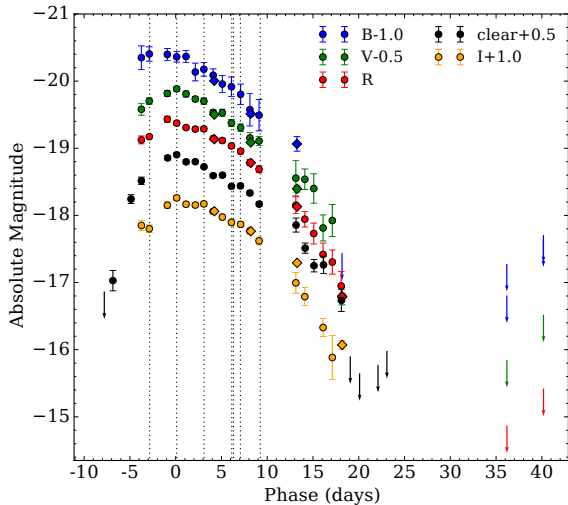


Figure 11. The KAIT and Nickel light curves of SN 2015U after correcting for MW dust absorption and host absorption. Nickel data are indicated with diamonds and KAIT data with circles, and the dates of our spectral observations are indicated with dashed vertical lines. We apply vertical offsets to every passband but *R*, to enable comparisons.

3.4 Comparisons with Other Supernovae

In Figure 12 we compare the light curves of SN 2015U to the *R*-band light curves of SN 2002bj (Poznanski et al. 2010), which was very similar though ~ 1 mag fainter, and SN 2010X (Kasliwal et al. 2010), which also matches well but was another ~ 1.5 mag fainter. SNLS04D4ec and SNLS06D1hc, two of the rapidly rising transients discovered by the Supernova Legacy Survey (SNLS) and presented by Arcavi et al. (2015), also show similar light-curve behaviour but ~ 0.5 mag brighter than SN 2015U (see their Figure 2). In Figure 13 we compare the spectra of these events: SN 2002bj was hydrogen deficient (SN I Ib-like, though not a good spectroscopic match to normal SNe I Ib) with a strong blue continuum and P-Cygni features at higher velocities than observed in SN 2015U, while SN 2010X showed no hydrogen (SN Ib/c-like, though again not a good spectroscopic match to normal SNe Ib/c) with broad absorption features. (Unfortunately, no spectra were obtained of the SNLS events.)

The light curves and spectra of SN 2015U are also quite similar to those of the rapidly evolving and luminous transients discovered in the PS1 dataset and presented by Drout et al. (2014). Figure 11 includes the *g* and *i*-band light curves of the relatively well-observed PS1-12bv from that sample; it was discovered at $z = 0.405$, so the *g* and *i* passbands probe rest wavelengths around 3500 \AA (about 100 \AA shortward of *B*) and 5350 \AA (similar to *V*), respectively. Without the 0.5 mag offset used in Figure 11, the *i*-band light curve of PS1-12bv would overlie the *V* band of SN 2015U almost exactly, and the *g*-band curve would be somewhat brighter than the *B* band of SN 2015U. There are no clear detections of any emission features in the spectrum of PS1-12bv, but it and the other events from the PS1 sample were discovered

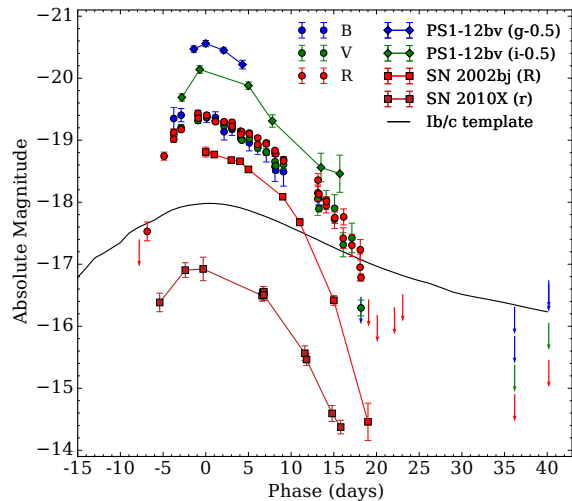


Figure 12. The extinction-corrected *BVR* light curves of SN 2015U compared to light curves of SNe 2002bj and 2010X (Poznanski et al. 2010; Kasliwal et al. 2010) and one of the rapidly evolving events from the PS1 sample (Drout et al. 2014). We also show the *R*-band SN Ib/c template from Drout et al. (2011) in black. Note that we group KAIT *clear*-band observations of SN 2015U with those in the *R* band.

at very large distances, and high-SNR spectra do not exist for those events. It is plausible that narrow emission lines of helium (and/or hydrogen) were present but went undetected.

Figure 13 shows that SN 2015U shares the blue colour and prominent He I emission features of the canonical SN Ib/c 2006jc (e.g., Foley et al. 2007; Pastorello et al. 2008). However, SN 2006jc was discovered post-peak and evolved more slowly than SN 2015U: the earliest extant spectrum of SN 2006jc was taken after the event had faded ~ 1 mag from peak and the spectrum had already transitioned into a nearly nebular phase, though a blue pseudocontinuum was apparent due to ongoing interaction with the CSM (Foley et al. 2007). In contrast, SN 2015U presented a continuum-dominated spectrum through our last epoch of spectroscopy, also taken after the event had faded ~ 1 mag from peak. Unlike SN 2015U, the light curve of SN 2006jc showed a tail out to 60+ days (fading somewhat faster than the $0.0098 \text{ mag day}^{-1}$ expected from fully trapped ^{56}Co decay; Foley et al. 2007).

The early-time spectrum of SN 2015U is similar to the very early spectra of SN II in 1998S, excepting the absence of hydrogen in the former. Both events show a smooth, blue, and (approximately) blackbody continuum. The He I lines of SN 2015U are stronger than those of SN 1998S, and the implied CSM velocity of SN 2015U is significantly higher, but the N III/C III complex near 4500 \AA is clearly detected in both. This feature dominates at very early times but disappears by peak (though that evolution took place over different timescales for these two SNe).

The ~ 20 -day timescale for SN 2015U's evolution and the increasing decline rate are reminiscent of the light curves expected for low- ^{56}Ni explosions in helium-dominated or

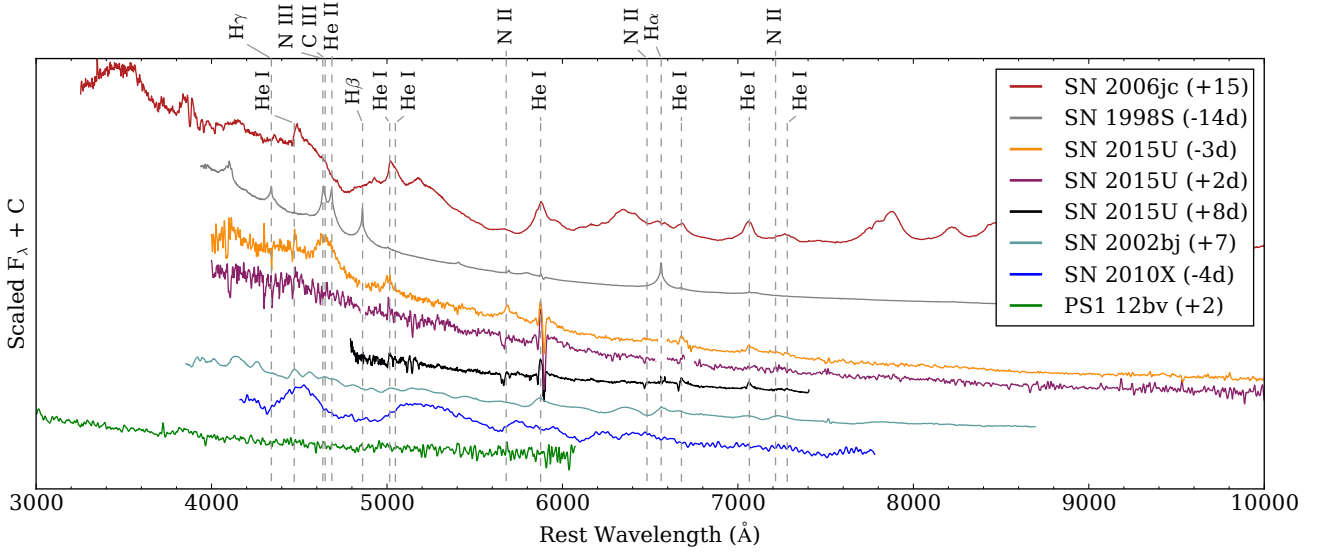


Figure 13. Spectra of SN 2015U compared with spectra of the prototypical SN Ibn 2006jc (Foley et al. 2007), the young SN IIn 1998S (Leonard et al. 2000; Shivvers et al. 2015), the rapidly fading SNe 2002bj and 2010X (Poznanski et al. 2010; Kasliwal et al. 2010), and one of the rapidly fading events from the PS1 sample (Drout et al. 2014). Galactic emission features have been masked in the low-resolution spectra of SN 2015U to facilitate comparisons.

oxygen-dominated envelopes — see, for example, the models of Dessart et al. (2011) and Kleiser & Kasen (2014). In these models, the recombination of helium or oxygen produces a dramatic and rapid drop in opacity within the ejecta and an inward-moving recombination front. SN 2015U was much more luminous than these models, but perhaps it was an analogous event wherein a recombination wave in the extended CSM produced a rapid fade from maximum luminosity as the CSM cools after shock breakout. Similar situations have been observed in hydrogen-rich SNe: there exists a subclass of SNe IIn that shows light curves with a plateau likely produced via hydrogen recombination within their extended CSM (SNe 1994W, 2009kn, and 2011ht; e.g., Mauerhan et al. 2013).

The narrow P-Cygni profiles and strong continua of SN 2015U’s spectra are clear indications of dense CSM. The diversity of ways in which such CSM can affect the light curves of SNe have been explored in detail by several authors motivated by observations of SNe IIn/Ibn, superluminous SNe, and rapidly fading SNe (e.g., Ofek et al. 2010; Chevalier & Irwin 2011; Kleiser & Kasen 2014), and comparisons of SN 2015U’s light curve to these models implies that SN 2015U was a shock-breakout event. The high luminosity indicates that shock breakout occurred at a large radius and that a significant fraction of the SN’s kinetic energy was converted into light, while the lack of a long-lasting light-curve tail shows that the CSM surrounding SN 2015U was more shell-like than wind-like (there is no interaction-powered tail) and that relatively little ^{56}Ni was produced (there is no radioactively powered tail).

The rapidly fading light curves of SNe 2002bj and 2010X are remarkably similar to those of SN 2015U, and we argue that their spectral differences do not exclude the possibility that these three events were fundamentally quite similar. By varying the radius of a putative opaque CSM

shell in a simple model, we can understand events spanning a range of luminosities and timespans for which the opaque CSM reprocesses the SN flux. Under the assumption that their light curves are all shock cooling curves without significant contribution from radioactive nickel, the peak luminosities and timescales of these three SNe should be governed roughly by

$$t_{\text{SN}} \propto E^{-1/6} M^{1/2} R^{1/6} \kappa^{1/6} T^{-2/3},$$

$$L_{\text{SN}} \propto E^{5/6} M^{-1/2} R^{2/3} \kappa^{-1/3} T^{4/3},$$

following Kleiser & Kasen (2014), adapted from Kasen & Woosley (2009) for hydrogen-free SNe and based on the analytic framework of Popov (1993). E is the energy of the SN explosion, M is the mass ejected, and R is the effective radius (in this case, the radius reached by a significant amount of mass ejected prior to the final explosion).

In particular, consider the peak-luminosity equation, assuming these explosions are similar in all their properties except for the effective pre-SN radius R , which would be determined by the time before explosion and the speed at which any pre-SN material was ejected. Inverting the equation, the pre-SN $R \propto L_{\text{SN}}^{3/2}$. If we assume that the ejecta velocities of all three objects are similar, this means that the ejecta from the SN itself will pass through the surrounding CSM in a time $t_{\text{interact}} \propto R$, and the length of time after explosion we expect to see narrow lines from this interaction is proportional to R . Comparing the relative peak luminosities, we find that, since SN 2015U exhibited narrow lines at least up to ~ 16.5 days after explosion, SN 2002bj should have shown narrow lines at least until ~ 5.5 days after explosion and the even dimmer SN 2010X would have shown narrow lines at least until ~ 0.52 days. These times are well before the first spectra were taken of either SN 2002bj or SN 2010X. Typically, we expect that to discover narrow lines in these

rapidly fading SNe, we will either need to look at the brightest among them or catch them very early. The luminosity (and timescale) may also depend on the explosion energies, ejected masses, and other properties of the SN, but these must be disentangled with more sophisticated numerical approaches.

3.5 Temperature and Luminosity Evolution

The extreme and uncertain degree of host-galaxy dust reddening toward SN 2015U makes estimating bolometric properties quite difficult. In §3.1 we assume that the emission from SN 2015U is roughly blackbody in spectral shape; here we further discuss this assumption. It has long been known that the continua of young SNe II exhibit “diluted blackbody” spectral energy distributions (SEDs), which (at optical wavelengths) are similar to the Planck function at a lower temperature (e.g., [Hershkowitz et al. 1986](#); [Eastman et al. 1996](#)). Though SN 2015U is certainly not a SN II, it is continuum-dominated, and in the sections above we present evidence that SN 2015U was shrouded in an optically thick CSM. In addition, [Moriya et al. \(2011\)](#) show that modeled shock breakouts from the hydrogen-dominated CSM around red supergiants exhibit roughly blackbody SEDs. [Rabinak & Waxman \(2011\)](#) explore shock breakouts from He or He/CO stellar envelopes in detail; for He-dominated stellar envelopes, they show that the colour temperature of the system deviates from the photosphere’s temperature by a (time-dependent) factor of only $\sim 20\%$, largely owing to diffusion effects as a helium recombination wave moves through the material.

Given the above discussion, we assume that SN 2015U’s emission was roughly blackbody and we estimate the bolometric properties by fitting a dust-reddened Planck spectrum to our multiband photometry. Using our almost nightly observations of SN 2015U in the *BVRI* passbands, we assembled the observed optical SEDs from -5 d to $+20$ d and find the best-fit blackbody temperature, radius, and luminosity using MCMC maximum-likelihood methods. As described in §3.1, there are large uncertainties in the properties of the host galaxy’s dust, and these uncertainties produce similarly large uncertainties in the absolute value of the temperature at any given time. In addition, our optical photometry largely probes the Rayleigh-Jeans tail of SN 2015U’s SED, so the implied bolometric corrections are large and uncertain. Our MCMC-produced error bars include these effects, and our photometric data do indicate significant temperature evolution (assuming $E(B - V)$ and R_V do not change). Because our data constrain the evolution of SN 2015U more strongly than they constrain the absolute values of any given parameter, it is useful to consider the implications for a few assumed values of $E(B - V)$.

Figure 14 shows the blackbody temperature, bolometric luminosity, and radius evolution of SN 2015U for three different assumed values of $E(B - V)$, adopting $R_V = 2.1$. In all cases, the best-fit temperature decreases over time, with the temperature falling rapidly before (optical) peak and then decreasing slowly thereafter. The effective blackbody radius increases with a photospheric velocity of $v_{\text{phot}} \approx 15,000 \text{ km s}^{-1}$ until peak, leveling off thereafter. Though this value of v_{phot} is similar to the characteristic velocities of ejecta in stripped-envelope SNe, our spectra do not show any material moving

Table 3. Bolometric Properties of SN 2015U

$E(B - V)$ (mag)	L_{peak} (erg s^{-1})	E_{rad} (erg)	T_{peak} (K)	R_{peak} (cm)
0.5	7.3×10^{42}	9.3×10^{48}	8400	1.5×10^{15}
0.94	5.9×10^{43}	7.1×10^{49}	19,000	8.7×10^{14}
1.05	2.3×10^{44}	2.9×10^{50}	30,000	6.7×10^{14}

Bolometric luminosity, radiated energy, blackbody temperature, and blackbody radius for the three assumed values of $E(B - V)_{\text{host}}$ shown in Figure 14. $E(B - V) = 0.94$ mag is our preferred value, but the degree of dust reddening produced by the ISM of NGC 2388 is very uncertain (see §3.1). This uncertainty is the dominant source of error in this analysis, and the spread over these three values of $E(B - V)$ indicates the range. All values are estimated through simple polynomial fits to the curves shown in Figure 14. To calculate E_{rad} , we integrated from day -5 to day $+20$ (the timespan of our almost nightly multiband photometric coverage), and for the other parameters we show the value at V -band peak. Note that the bolometric luminosity may peak before the optical maximum; again, see Figure 14.

that quickly and, given our interpretation of SN 2015U as a cooling shock-breakout event, we expect the photospheric radius to be approximately constant throughout these observations. In addition, Figure 14 may surprise the reader by indicating that the peak bolometric luminosity occurred several days before the optical peak. These results indicate that our pre-maximum temperatures are perhaps overestimated (the bolometric corrections are at their largest and most uncertain at early times). Unfortunately, we do not know of any observations constraining the ultraviolet emission of SN 2015U.

However, we can constrain the temperature evolution of SN 2015U independently of the continuum shape, through the relative line strengths of detected emission lines in our spectra. Though detailed modeling is beyond the scope of this paper, the pre-maximum detection and rapid fading of the N III/C III/He II 4500 Å complex in our spectra of SN 2015U brings to mind the spectral evolution of SN 1998S (see Figure 13). Detailed CMFGEN models of SN 1998S while the 4500 Å feature was strong were presented by [Shivvers et al. \(2015\)](#), indicating a temperature of $\sim 30,000$ K throughout most of the line-forming region. The agreement between this value and the pre-maximum temperatures found for SN 2015U assuming $E(B - V) = 0.94$ mag are heartening. In Table 3 we present the integrated energy released and various values at V -band peak.

3.6 Nickel Content

A ^{56}Ni -powered tail has been detected in some SNe Ibn, but many members of this subclass (including SN 2015U) do not show one (e.g., [Foley et al. 2007](#); [Gorbikov et al. 2014](#); [Pastorello et al. 2016](#)). For most SNe I, Arnett’s law can be used to estimate the total ^{56}Ni synthesized by the explosion ([Arnett 1982](#)). That approach is not applicable for shock-breakout events (or events powered by ongoing CSM interaction), and so we only place an upper limit on the amount of ^{56}Ni present in SN 2015U based upon our nondetection of a radioactive tail. We use the method of [Hamuy \(2003\)](#): given a luminosity L_t at time t and an explosion time t_0 , and

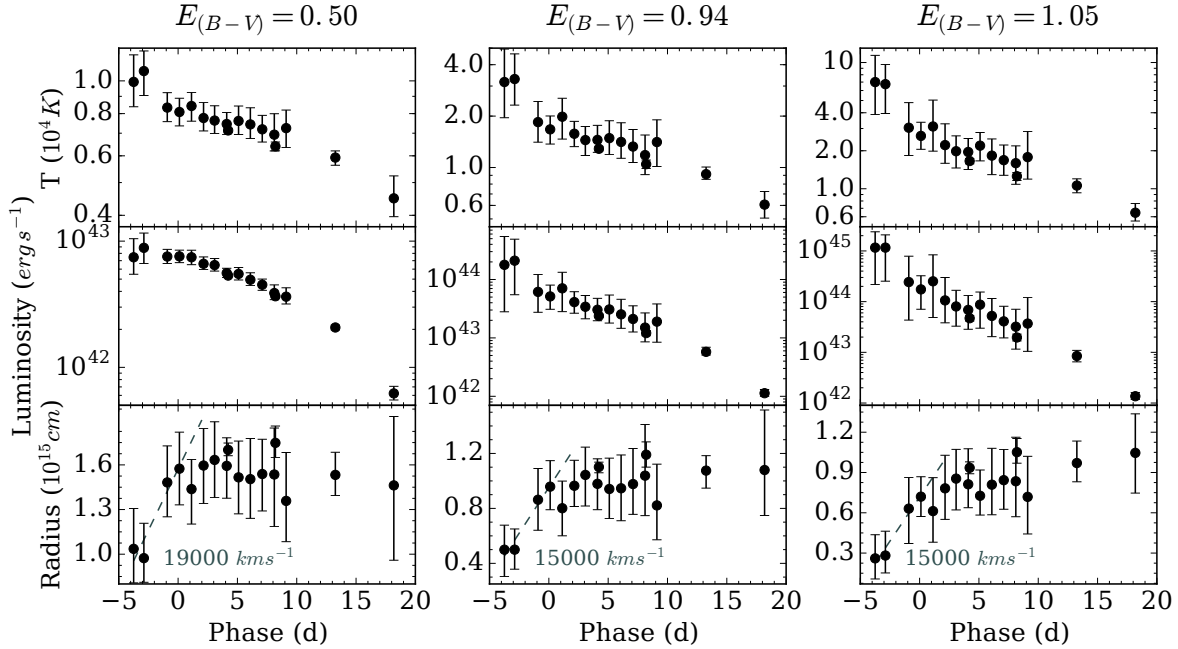


Figure 14. The best-fit blackbody temperature, bolometric luminosity, and radius evolution of SN 2015U for three assumed values of $E(B-V)$ as a function of phase relative to V -band peak. The leftmost column shows the evolution assuming a value of 0.5 mag, the middle column assumes our preferred value of 0.94 mag, and the rightmost column corresponds to a value of 1.05 mag. In the lower panels, we show linear fits to the radius evolution up to V -band peak with a grey dashed line. All parameters are fitted using maximum-likelihood MCMC methods and error bars represent 95% confidence intervals (but do not include errors caused by uncertainty in the degree of host-galaxy dust reddening).

assuming complete γ -ray trapping,

$$M_{\text{Ni}} = (7.866 \times 10^{44}) L_t \exp\left(\frac{(t-t_0)/(1+z) - 6.1}{111.26}\right) M_{\odot}$$

Our most constraining observation of this tail is a non-detection in the R band at +36 days. Our last multiband photometric measurement of the temperature yields $T = 6000 \pm 1000$ K at +18 d (see §3.5). We adopt that temperature to calculate the blackbody luminosity for a source at our nondetection threshold, but we note that the temperature is still changing at this time, possibly affecting our results. This calculation yields an upper limit of $M_{\text{Ni}} \lesssim 0.019 M_{\odot}$ — quite low for SNe I ($M_{\text{Ni, Ia}} \gtrsim 0.4 M_{\odot}$, $M_{\text{Ni, Ib/c}} \approx 0.2 M_{\odot}$; Contardo et al. 2000; Drout et al. 2011), but within the range of values observed for SNe II ($M_{\text{Ni, II}} \approx 0.0016$ – $0.26 M_{\odot}$; Hamuy 2003).

3.7 Progenitor Mass-Loss Rate

We adopt the simple shock-wind interaction model of Chevalier & Irwin (2011) to estimate the properties of the CSM surrounding SN 2015U. We assume that the CSM is spherically symmetric and follows a wind-like density profile ($\rho \propto r^{-2}$), and we use the opacity of helium-dominated material in our calculations ($\kappa = 0.2 \text{ cm}^2 \text{ g}^{-1}$). Margutti et al. (2014) solve the Chevalier & Irwin (2011) model in terms of three observables: break-out radius R_{bo} (the radius at which radiation diffuses forward ahead of the shock), total radiated energy E_{rad} , and light-curve rise time t_{rise} . We use $t_{\text{rise}} = 9$ days and, assuming $E(B-V)_{\text{host}} = 0.94$ mag, we adopt $E_{\text{rad}} = 7.1 \times 10^{49}$ erg

from Table 3. For R_{bo} we adopt the first measured blackbody radius from Figure 14: $R_{\text{bo}} = 5 \times 10^{14}$ cm. The resultant mass-loss estimate is very large, $\dot{M} \approx 1.2 M_{\odot} \text{ yr}^{-1}$. However, in this model $\dot{M} \propto R_{\text{bo}}^{-3}$, and there is reason to believe that our measurement of the blackbody radius before peak brightness does not reflect the true R_{bo} (see §3.5). If we instead use $R_{\text{bo}} = 9 \times 10^{14}$ cm, the blackbody radius at V -band peak, we calculate $\dot{M} \approx 0.2 M_{\odot} \text{ yr}^{-1}$.

Both of these values are several orders of magnitude above the most extreme mass-loss rates produced by steady winds from stars, but they are not far from the time-averaged eruptive mass-loss rates from luminous blue variables (LBVs, which may well exhibit much higher instantaneous mass-loss rates; Smith 2014). Observations of iPTF13beo, a recent SN Ibn discovered by the intermediate Palomar Transient Factory (PTF), implied an even higher (but short-lived) mass-loss rate of $\dot{M} \approx 2.4 M_{\odot} \text{ yr}^{-1}$ immediately before the progenitor underwent core collapse (estimated via similar methods; Gorbikov et al. 2014).

If the CSM around SN 2015U was launched from the surface explosively rather than through a steady wind, the assumption that $\rho_{\text{CSM}} \propto r^{-2}$ is suspect. In fact, the lack of an interaction-powered tail in the light curve of SN 2015U indicates that the density profile cannot be wind-like: Chevalier & Irwin (2011) show that ongoing interaction with a wind-like CSM powers a tail with $L \propto t^{-0.6}$, and SN 2015U fades more rapidly than that throughout its post-peak evolution. The lack of any high-velocity features in our spectra argues that this outer CSM must be optically thick at least out to the radius of the shock at the time of our last spec-

trum. Assuming $v_{\text{shock}} \approx 20,000 \text{ km s}^{-1}$, the velocity of the fastest material in unshrouded stripped-envelope SNe, this produces an estimate for the CSM extent of $R \gtrsim 3 \times 10^{15} \text{ cm}$. Adopting the average He I velocity measured from our spectra (745 km s^{-1}), material at that radius was launched 1–2 yr before core collapse. However, it is likely that the SN ejecta is slowed by its collision with the CSM, and so it may be more physically relevant to assume the CSM extent to be $R \gtrsim 9 \times 10^{14} \text{ cm}$ (the blackbody radius at V-band peak); material at that radius was launched $< 1 \text{ yr}$ before collapse.

It is not clear whether the extreme mass loss from SN 2015U’s progenitor was episodic and brief or sustained over a year or more, nor is it known whether the assumption of spherical symmetry is appropriate. We leave a more thorough examination of these questions to future work.

3.8 Constraints on Progenitor Variability

The presence of dense CSM suggests a recent history of extreme mass loss and perhaps variability of the progenitor star. SN Ibn 2006jc, for example, underwent a bright outburst ($M = -14 \text{ mag}$) about 2 yr before becoming a genuine SN (Nakano et al. 2006; Foley et al. 2007; Pastorello et al. 2007), and there are multiple cases where the progenitors of SNe II_n have been detected in outburst in the years prior to core collapse (e.g., Ofek et al. 2014). KAIT has been monitoring NGC 2388 for almost 20 yr and we searched this extensive dataset for evidence of pre-explosion variability. We augment our unfiltered KAIT data with the publicly available PTF images of the field in the r passband.⁹

Examining 758 images with observed upper limits fainter than 17.0 mag from 1998 Oct. through 2015 Feb. 10, we find no evidence for previous outbursts of the progenitor based upon difference imaging (using one of our deepest single exposures for a template). We stacked our images into rolling-window time bins 20 d wide and subtracted templates to search for evidence of previous outbursts of that timescale, but found none. We also stacked all images together and searched for evidence of a progenitor, but found none. (Note that we stacked the KAIT and PTF images separately, and we did not perform difference imaging on these very deep stacks, as we had no templates with which to compare.) Figure 15 plots our 1σ single-image nondetections and the observed light curve of SN 2015U.

Though we have regular imaging of NGC 2388 most years since 1998, the field was inaccessible to our telescopes for several months every year, so there are significant gaps, especially compared to the timescale of SN 2015U’s light curve ($\sim 20 \text{ d}$). The orange bars along the bottom of Figure 15 mark every night at which more than 20 days had passed since the previous upper limit, indicating timespans when a previous SN 2015U-like event could have occurred undetected.

Unfortunately, even the epochs that were covered by our monitoring campaigns do not yield stringent constraints on the luminosity of a previous outburst, partially owing to the estimated $\sim 1.5 \text{ mag}$ of host-galaxy dust extinction along the line of sight toward SN 2015U. The detected outburst of SN 2006jc’s precursor reached a peak of $M_r \approx -14.1 \text{ mag}$

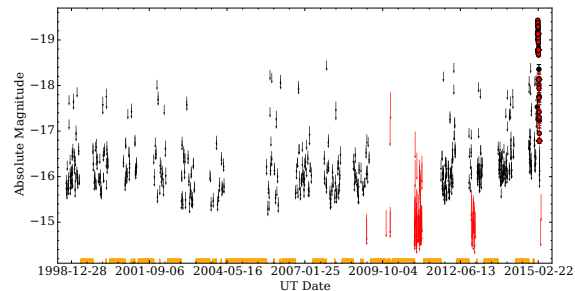


Figure 15. Our 1σ nondetections from KAIT unfiltered images (black) and PTF R images (red). The light curve of SN 2015U is shown to the far right. Timespans for which no upper limit had been obtained for at least 20 days are marked in orange along the bottom.

(Pastorello et al. 2007), and such an outburst in SN 2015U’s precursor would have probably remained undetected by our monitoring campaign.

4 CONCLUSION

In this paper we presented observations of SN 2015U, a highly extinguished, low-velocity, rapidly evolving, luminous, apparently hydrogen-free SN which exploded in the strongly star-forming galaxy NGC 2388. Though detailed modeling has yet to be performed, and the degree of host-galaxy dust interference is uncertain, our observations indicate that SN 2015U was a core-collapse SN with a peak powered by shock breakout from a dense CSM rather than radioactive decay. We suggest that this CSM was not wind-like but was instead created by at least one extreme episode of mass loss ($\dot{M} \approx 0.2\text{--}1.2 M_{\odot} \text{ yr}^{-1}$) within a few years of core collapse. The CSM that surrounded SN 2015U was effectively hydrogen-free but was helium-rich; we also detect features from nitrogen, iron, and probably carbon in our spectra. No long-lasting light-curve tail was observed from radioactivity or from ongoing CSM interaction, thereby constraining the amount of ^{56}Ni that could have been produced in SN 2015U to $\lesssim 0.019 M_{\odot}$.

SN 2015U is a remarkably well-observed SN Ibn, especially among the rapidly fading subset of these events, and we find many similarities between it and other SNe in the literature. Modern surveys indicate the existence of a class of blue, continuum-dominated, hydrogen-deficient, luminous, and rapidly evolving SNe including those found by Drout et al. (2014) and Arcavi et al. (2015); our analysis of SN 2015U implies fundamental similarities between these events, a subset of the SNe Ibn (e.g., Pastorello et al. 2016), and other rapidly fading SNe of lower luminosity (i.e., SNe 2002bj and 2010X). While the exact progenitors of these events are quite uncertain, it is clear that they demand extreme mass-loss rates from their stripped-envelope progenitor stars.

⁹ <http://irsa.ipac.caltech.edu/applications/ptf/>

ACKNOWLEDGEMENTS

The authors thank M. Drout, R. Foley, P. Nugent, D. Kasen, E. Quataert, D. Poznanski and O. Fox for useful comments and discussions. We thank the *HST*, Keck Observatory, and Lick Observatory staffs for their expert assistance with the observations. We also thank the following Nickel 1m observers and KAIT checkers for their valuable assistance with this work: A. Bigley, C. Gould, G. Halevi, K. Hayakawa, A. Hughes, H.J. Kim, M. Kim, P. Lu, K. Pina, T. Ross, S. Stegman, and H. Yuk.

A.V.F.'s supernova research group at U. C. Berkeley is supported by NSF grant AST-1211916, the TABASGO Foundation, Gary and Cynthia Bengier, and the Christopher R. Redlich Fund. Additional assistance is provided by NASA/*HST* grants AR-14295 and GO-14149 from the Space Telescope Science Institute, which is operated by the Association of Universities for Research in Astronomy, Inc., under NASA contract NAS5-26555. J.M.S. is supported by an NSF Astronomy and Astrophysics Postdoctoral Fellowship under award AST-1302771.

Some of the data presented herein were obtained at the W. M. Keck Observatory, which is operated as a scientific partnership among the California Institute of Technology, the University of California, and NASA; the observatory was made possible by the generous financial support of the W. M. Keck Foundation. KAIT and its ongoing operation were made possible by donations from Sun Microsystems, Inc., the Hewlett-Packard Company, AutoScope Corporation, Lick Observatory, the NSF, the University of California, the Sylvia and Jim Katzman Foundation, and the TABASGO Foundation. Research at Lick Observatory is partially supported by a generous gift from Google. This research was based in part on data taken with the NASA/ESA *Hubble Space Telescope*, and obtained from the Hubble Legacy Archive, which is a collaboration between the Space Telescope Science Institute (STScI/NASA), the Space Telescope European Coordinating Facility (ST-ECF/ESA), and the Canadian Astronomy Data Centre (CADM/NRC/CSA). This research has made use of the NASA/IPAC Extragalactic Database (NED) which is operated by the Jet Propulsion Laboratory, California Institute of Technology, under contract with NASA.

REFERENCES

- Anderson J. P., et al., 2014, *ApJ*, **786**, 67
 Anupama G. C., Sivarani T., Pandey G., 2001, *A&A*, **367**, 506
 Arcavi I., et al., 2012, *ApJ*, **756**, L30
 Arcavi I., et al., 2015, preprint, ([arXiv:1511.00704](https://arxiv.org/abs/1511.00704))
 Arnett W. D., 1982, *ApJ*, **253**, 785
 Auer L. H., van Blerkom D., 1972, *ApJ*, **178**, 175
 Bianco F. B., et al., 2014, *ApJS*, **213**, 19
 Brocklehurst M., 1971, *MNRAS*, **153**, 471
 Cardelli J. A., Clayton G. C., Mathis J. S., 1989, *ApJ*, **345**, 245
 Chevalier R. A., Irwin C. M., 2011, *ApJ*, **729**, L6
 Chugai N. N., 2001, *MNRAS*, **326**, 1448
 Clayton G. C., Mathis J. S., 1988, *ApJ*, **327**, 911
 Contardo G., Leibundgut B., Vacca W. D., 2000, *A&A*, **359**, 876
 Coyne G. V., Gehrels T., 1966, *AJ*, **71**, 355
 Dessart L., Hillier D. J., Livne E., Yoon S.-C., Woosley S., Waldman R., Langer N., 2011, *MNRAS*, **414**, 2985
 Dessart L., Hillier D. J., Woosley S., Livne E., Waldman R., Yoon S.-C., Langer N., 2015, *MNRAS*, **453**, 2189
 Drout M. R., et al., 2011, *ApJ*, **741**, 97
 Drout M. R., et al., 2013, *ApJ*, **774**, 58
 Drout M. R., et al., 2014, *ApJ*, **794**, 23
 Eastman R. G., Schmidt B. P., Kirshner R., 1996, *ApJ*, **466**, 911
 Faber S. M., et al., 2003, in Iye M., Moorwood A. F. M., eds, *Society of Photo-Optical Instrumentation Engineers (SPIE) Conference Series Vol. 4841, Instrument Design and Performance for Optical/Infrared Ground-based Telescopes*. pp 1657–1669, doi:10.1117/12.460346
 Fassia A., et al., 2001, *MNRAS*, **325**, 907
 Filippenko A. V., 1982, *PASP*, **94**, 715
 Filippenko A. V., 1991, in Danziger I. J., Kjaer K., eds, *European Southern Observatory Conference and Workshop Proceedings Vol. 37, European Southern Observatory Conference and Workshop Proceedings*. p. 343
 Filippenko A. V., 1997, *ARA&A*, **35**, 309
 Filippenko A. V., Li W. D., Treffers R. R., Modjaz M., 2001, in Paczynski B., Chen W.-P., Lemme C., eds, *Astronomical Society of the Pacific Conference Series Vol. 246, IAU Colloq. 183: Small Telescope Astronomy on Global Scales*. p. 121
 Foley R. J., Smith N., Ganeshalingam M., Li W., Chornock R., Filippenko A. V., 2007, *ApJ*, **657**, L105
 Fransson C., et al., 2014, *ApJ*, **797**, 118
 Friedman S. D., et al., 2011, *ApJ*, **727**, 33
 Gal-Yam A., 2012, *Science*, **337**, 927
 Gal-Yam A., et al., 2014, *Nature*, **509**, 471
 Ganeshalingam M., et al., 2010, *ApJS*, **190**, 418
 Gehrels T., Silvester A. B., 1965, *AJ*, **70**, 579
 Gorbikov E., et al., 2014, *MNRAS*, **443**, 671
 Hamuy M., 2003, *ApJ*, **582**, 905
 Herbig G. H., 1995, *ARA&A*, **33**, 19
 Hershkowitz S., Linder E., Wagoner R. V., 1986, *ApJ*, **301**, 220
 Hillier D. J., 1991, *A&A*, **247**, 455
 Kasen D., Woosley S. E., 2009, *ApJ*, **703**, 2205
 Kasliwal M. M., et al., 2010, *ApJ*, **723**, L98
 Khazov D., et al., 2016, *ApJ*, **818**, 3
 Kleiser I. K. W., Kasen D., 2014, *MNRAS*, **438**, 318
 Kumar S., Yuk H., Zheng W., Filippenko A. V., 2015, *Central Bureau Electronic Telegrams*, 4164, 1
 Lan T.-W., Ménard B., Zhu G., 2015, *MNRAS*, **452**, 3629
 Leonard D. C., Filippenko A. V., Barth A. J., Matheson T., 2000, *ApJ*, **536**, 239
 Li W., Filippenko A. V., Chornock R., Jha S., 2003, *PASP*, **115**, 844
 Liu Y.-Q., Modjaz M., Bianco F. B., Graur O., 2015, preprint, ([arXiv:1510.08049](https://arxiv.org/abs/1510.08049))
 Margutti R., et al., 2014, *ApJ*, **780**, 21
 Matheson T., 2001, *PASP*, **113**, 1155
 Matheson T., et al., 2000, *AJ*, **120**, 1487
 Matheson T., Filippenko A. V., Li W., Leonard D. C., Shields J. C., 2001, *AJ*, **121**, 1648
 Mauerhan J. C., et al., 2013, *MNRAS*, **431**, 2599
 Mauerhan J. C., et al., 2015, *MNRAS*, **453**, 4467
 Milisavljevic D., et al., 2015, *ApJ*, **815**, 120
 Miller J., Stone R., 1993, *Lick Observatory Technical Reports*, 66
 Modjaz M., et al., 2014, *AJ*, **147**, 99
 Moriya T., Tominaga N., Blinnikov S. I., Baklanov P. V., Sorokina E. I., 2011, *MNRAS*, **415**, 199
 Nachman P., Hobbs L. M., 1973, *ApJ*, **182**, 481
 Nakano S., Itagaki K., Puckett T., Gorelli R., 2006, *Central Bureau Electronic Telegrams*, 666, 1
 Ochner P., et al., 2015, *The Astronomer's Telegram*, **7105**, 1
 Ofek E. O., et al., 2010, *ApJ*, **724**, 1396
 Ofek E. O., et al., 2014, *ApJ*, **789**, 104
 Pastorello A., et al., 2007, *Nature*, **447**, 829
 Pastorello A., et al., 2008, *MNRAS*, **389**, 113

- Pastorello A., et al., 2015, *MNRAS*, 454, 4293
- Pastorello A., et al., 2016, *MNRAS*, 456, 853
- Patat F., et al., 2015, *A&A*, 577, A53
- Pereira-Santaella M., et al., 2015, *A&A*, 577, A78
- Pérez F., Granger B. E., 2007, *Computing in Science and Engineering*, 9, 21
- Phillips M. M., et al., 2013, *ApJ*, 779, 38
- Popov D. V., 1993, *ApJ*, 414, 712
- Poznanski D., et al., 2010, *Science*, 327, 58
- Poznanski D., Prochaska J. X., Bloom J. S., 2012, *MNRAS*, 426, 1465
- Rabinak I., Waxman E., 2011, *ApJ*, 728, 63
- Riess A. G., et al., 1999, *AJ*, 118, 2675
- Sanders N. E., et al., 2015, *ApJ*, 799, 208
- Schlafly E. F., Finkbeiner D. P., 2011, *ApJ*, 737, 103
- Schlegel E. M., 1990, *MNRAS*, 244, 269
- Serkowski K., Mathewson D. S., Ford V. L., 1975, *ApJ*, 196, 261
- Shivvers I., Groh J. H., Mauerhan J. C., Fox O. D., Leonard D. C., Filippenko A. V., 2015, *ApJ*, 806, 213
- Silverman J. M., et al., 2012, *MNRAS*, 425, 1789
- Silverman J. M., et al., 2013a, *ApJS*, 207, 3
- Silverman J. M., et al., 2013b, *ApJ*, 772, 125
- Smith N., 2014, *ARA&A*, 52, 487
- Somerville W. B., 1988, *The Observatory*, 108, 44
- Stetson P. B., 1987, *PASP*, 99, 191
- Strömgren B., 1948, *ApJ*, 108, 242
- Tsvetkov D. Y., Volkov I. M., Pavlyuk N. N., 2015, *Information Bulletin on Variable Stars*, 6140, 1
- Whittet D. C. B., Martin P. G., Hough J. H., Rouse M. F., Bailey J. A., Axon D. J., 1992, *ApJ*, 386, 562
- Wright E. L., 2006, *PASP*, 118, 1711
- Yaron O., Gal-Yam A., 2012, *PASP*, 124, 668
- de Vaucouleurs G., de Vaucouleurs A., Corwin Jr. H. G., Buta R. J., Paturel G., Fouqué P., 1991, *Third Reference Catalogue of Bright Galaxies. Volume I: Explanations and references. Volume II: Data for galaxies between 0^h and 12^h. Volume III: Data for galaxies between 12^h and 24^h.*

This paper has been typeset from a $\text{\TeX}/\text{\LaTeX}$ file prepared by the author.